

Article

Adsorption of Lead (II) Ions onto Goethite Chitosan Beads: Isotherms, Kinetics, and Mechanism Studies

Tanawit Sirijaree ^{1,2} and Pornsawai Praipipat ^{1,2,*}¹ Department of Environmental Science, Faculty of Science, Khon Kaen University, Khon Kaen 40002, Thailand² Environmental Applications of Recycled and Natural Materials (EARN) Laboratory, Khon Kaen University, Khon Kaen 40002, Thailand

* Correspondence: pornprai@kku.ac.th

Abstract: Lead is a highly toxic heavy metal that creates a water pollutant. It can be released from industrial processes, agricultural chemistry, and community wastes, affecting creatures and human health even at a low concentration. As a result, it is advised that lead be removed before releasing wastewater into the environment. This study synthesized three chitosan bead materials from shrimp shell wastes which were chitosan powder beads (CB), chitosan powder mixed with goethite beads (CFB), and chitosan powder beads coated with goethite (CBF) for removing lead in an aqueous solution. Their surface area, pore volumes, and pore sizes were explored according to Brunauer–Emmett–Teller, and their crystalline formations were investigated using an X-ray diffractometer. Their surface structures were studied using field emission scanning electron microscopy and a focus ion beam, and their chemical compositions were determined using an energy dispersive X-ray spectrometer. Their chemical functional groups were identified via Fourier-transform infrared spectroscopy. In addition, batch experiments were conducted to investigate the effects of several factors on removing lead, and the adsorption isotherm and kinetics were also investigated for determining their adsorption pattern and mechanism. In addition, the desorption experiments were studied to confirm their possible material reusability. The CBF demonstrated the highest surface area and smallest pore size compared with the other materials. In addition, the pore sizes of the CFB and CBF were micropores, whereas those of the CB were mesopores. All materials were semicrystalline structures, and the specific goethite peaks were observed in the CFB and CBF. All materials had spherical shapes with heterogeneous surfaces. Six chemical components of O, C, Ca, N, Cl, and Na were discovered in all materials, and Fe was only found in the CFB and CBF because of the addition of goethite. Five main chemical functional groups of N–H, O–H, C–H, C–O, and –COOH were found in all materials. The optimum conditions of the CB, CFB, and CBF for removing lead were 0.5 g, 16 h, pH 5, 0.5 g, 16 h, pH 5, and 0.4 g, 14 h, pH 5, respectively. The results of the batch experiments demonstrated that the CB, CFB, and CBF were high-efficiency adsorbents for removing lead in solution by more than 95%, whereby the CBF showed the highest lead removal of 99%. The Freundlich isotherm model and pseudo-second-order kinetic model helped to well explain their adsorption pattern and mechanism. The maximum lead adsorption capacities of the CB, CFB, and CBF were 322.58, 333.33, and 344.83 mg/g, respectively. Furthermore, all chitosan materials can be reused for more than three cycles with high lead removal by more than 94%; so, they are potential materials for application in industrial applications.



Citation: Sirijaree, T.; Praipipat, P. Adsorption of Lead (II) Ions onto Goethite Chitosan Beads: Isotherms, Kinetics, and Mechanism Studies. *ChemEngineering* **2023**, *7*, 52. <https://doi.org/10.3390/chemengineering7030052>

Academic Editors: Alirio E. Rodrigues and Andrew S. Paluch

Received: 3 February 2023

Revised: 26 April 2023

Accepted: 12 May 2023

Published: 1 June 2023



Copyright: © 2023 by the authors. Licensee MDPI, Basel, Switzerland. This article is an open access article distributed under the terms and conditions of the Creative Commons Attribution (CC BY) license (<https://creativecommons.org/licenses/by/4.0/>).

Keywords: food waste; chitosan; goethite; adsorption; lead ions; wastewater

1. Introduction

Heavy metal pollution in water is becoming a major environmental concern around the world because it can be released from an increasing number of industries; so, wastewater from pollutant sources varies depending on the type of industry [1,2]. Lead is the most widely used raw material in many industries such as batteries, paint and pigments,

petroleum, and ceramics [3]. Lead is highly toxic even at a low concentration and can affect organisms via bioaccumulation and biomagnification [4,5], including human health in the form of respiratory, gastrointestinal, and nervous system problems and carcinogens [6,7]. As a result, the World Health Organization (WHO) guideline for the clinical management of exposure to lead has specified provisional guidelines to address and prevent the effects of contamination and exposure to lead in drinking water at 10 µg/L [3], and the United States Environmental Protection Agency (USEPA) has established the maximum lead ion contaminant level in drinking water as being 0.015 mg/L [8].

At present, lead in wastewater is treated using several processes such as chemical precipitation, coagulation–flocculation, membrane filtration, adsorption, electrochemical treatment process, membrane separation process, ion exchange, photocatalysis, oxidation, and biological treatment [9,10]. However, before deciding to implement these methods, factors such as operation and disposal costs must be considered. As a result, adsorption is regarded as one of the most effective and intriguing strategies for increasing the efficiency of heavy metal removal in water [11–13]. The adsorption method depends on many factors, and one of the key factors is the adsorbent. As a result, the optimum adsorbent should have high removal efficiency and be specific to the pollutant being treated, while being inexpensive. For heavy metal removals, several adsorbents from commercial, natural, and waste sources are used, such as activated carbon, resin, silica, bagasse, lemon peel, rice husk, eggshells, creeps, and crustacean shells [14–19]. This is due to the increasing waste problem, especially food waste, which is a result of the increasing consumption of the population. Due to the increasing waste problem, especially food waste from the increasing consumption of the human population, the use of natural waste materials for new benefits is an interesting idea because this concept is useful for waste management, recycling waste, and treating wastewater. Among the food waste management options, an interesting choice is using crustacean and mollusk shell waste as raw materials for chitosan extraction and using the structure and properties of chitosan to remove heavy metals. Chitosan can remove several kinds of heavy metals from wastewater, including cadmium (Cd), copper (Cu), lead (Pb), arsenic (As), chromium (Cr), mercury (Hg), and nickel (Ni), according to previous studies [20–24]. However, investigations into how to improve the adsorption efficiency of chitosan specific to wastewater pollutants are still interesting.

Many previous studies have used various metal oxides of iron (II or III) oxide (Fe_3O_4 or Fe_2O_3), iron (III) oxide-hydroxide, zinc oxide (ZnO), titanium dioxide (TiO_2), magnesium oxide (MgO), aluminum oxide (Al_2O_3), manganese oxide (MnO), and goethite ($\text{FeO}(\text{OH})$) for improving the effectiveness of heavy metals, dye, or acid removals from wastewater because they increase surface area, pore volume, and the functional group of active sites [25–36]. Therefore, adding metal oxides to adsorbents promotes an increase in the efficiency of removing metal ions from wastewater, as similarly found in another report in Table 1. However, the direct use of metal oxides is not practical in industrial continuous flow systems due to clogging problems, pressure drops, and difficult separation after treatments [37,38]. To obtain high adsorption effectiveness for eliminating a particular target pollutant, it is therefore a good idea to add metal oxides to the effective adsorbent material. Additionally, the development of a long-lasting adsorbent form may aid in long-term use and reduce operating expenses. As a result, the goal of this study was to increase the effectiveness of chitosan material for lead removal from wastewater for upcoming industrial applications by including metal oxide and altering the material's form by employing shrimp shell waste as a raw material. The main objective of the present study was to synthesize chitosan beads modified with $\text{FeO}(\text{OH})$ (goethite), which were chitosan powder beads (CB), chitosan powder mixed with goethite beads (CFB), and chitosan powder beads coated with goethite (CBF), for removing lead from artificial wastewater. Their surface area, pore volumes, and pore sizes were explored according to Brunauer–Emmett–Teller, and their crystalline formations were investigated using an X-ray diffractometer. Their surface structures were studied via field emission scanning electron microscopy and the focus ion beam, and their chemical compositions were determined using an energy dispersive

X-ray spectrometer. Their chemical functional groups were identified via Fourier-transform infrared spectroscopy. Furthermore, batch experiments were performed to compare the efficacy of their lead removals, adsorption isotherms and kinetics were verified to know the properties of their adsorption, and the reuse potentials of the CB, CFB, and CBF were estimated via desorption experiments.

Table 1. Comparison of various adsorbents modified with metal oxides for heavy metal adsorptions.

Adsorbents	Metal Oxides	Metal Ions	Concentrations (mg/L)	q _{max} (mg/g)	References
Algae	Ferric chloride	Cr(VI)	80	69.77	[39]
		Cu(II)	80	38.68	
		Pb(II)	80	62.32	
		Cd(II)	80	42.12	
Eggshell	Iron(III) oxide-hydroxide	Pb(II)	50	42.74	[26]
Lemon peels	Iron(III) oxide-hydroxide	Pb(II)	50	5.67	[28]
Peanut shell	Hydrous ferric oxide	Cd(II)	35	29.90	[40]
		Cu(II)	35	34.10	
Pistachio shell	Ferric chloride hexahydrate	Pb(II)	80	147.05	[41]
		As(III)	80	151.51	
		Cd(II)	80	119.04	
Sugarcane bagasse	Iron(III) oxide-hydroxide	Pb(II)	50	57.47	[27]
Sawdust	Iron(III) oxide-hydroxide	Pb(II)	50	47.17	[42]
Zeolite A	Iron(III) oxide-hydroxide	Pb(II)	50	625	[29]
Zeolite A	Iron(III) oxide-hydroxide	Pb(II)	50	909.09	[43]
Bentonite	Ferric nitrate	Pb(II)	5.72	74.20	[44]
		Cd(II)	5.28	41.30	
		As(V)	6.74	5	
		Pb(II)	10	850	
Silica	Ferric nitrate	Cr(III)	10	770	[45]
		Cd(II)	10	690	
Chitosan	Magnetic iron oxides	Pb(II)	32.37	234.77	[46]
Chitosan	Zinc oxide	Pb(II)	50	47.34	[30]
Chitosan	Zinc oxide	Pb(II)	20	476.10	[47]
		Cd(II)	20	135.10	
Chitosan	Ferrous sulfate heptahydrate	Cu(II)	20	117.60	[48]
		Cu(II)	200	147	
		Hg(II)	20	338	

2. Materials and Methods

2.1. Chemicals

All chemicals were of analytical grade (AR) without purification before use. Chitosan ($\geq 75\%$ deacetylated) (Sigma-Aldrich, St. Louis, MO, USA) was used as the commercial chitosan standard (STD), along with sodium hydroxide (NaOH) (RCI Labscan, Bangkok, Thailand), sodium alginate ($\text{NaC}_6\text{H}_7\text{O}_6$)_n (Merck, Darmstadt, Germany), calcium chloride (CaCl_2) (Kemaus, Cherrybrook, Australia), 37% hydrochloric acid (HCl) (Merck, Germany), 65% nitric acid (HNO_3) (Merck, Germany), 30–63% goethite or iron hydroxide oxide ($\text{FeO}(\text{OH})$) (Merck, Darmstadt, Germany), and lead nitrate ($\text{Pb}(\text{NO}_3)_2$) (QR&C, New Zealand). For pH adjustments, 0.5 M NaOH and 0.5 M HNO_3 were used.

2.2. The Synthesis of Chitosan Powder (CP)

The synthesis of chitosan powder (CP) was modified from Ngamsurach, P. et al., 2022, Varun T.K. et al., 2017, Boudouaia N. et al., 2019, and Antonino R.S.C.M.D.Q. et al., 2017 [30,49–51], which included three steps which were demineralization, deproteinization, and deacetylation, as shown in Figure 1a; the details are provided in detail below:

Step 1: Raw materials' preparation

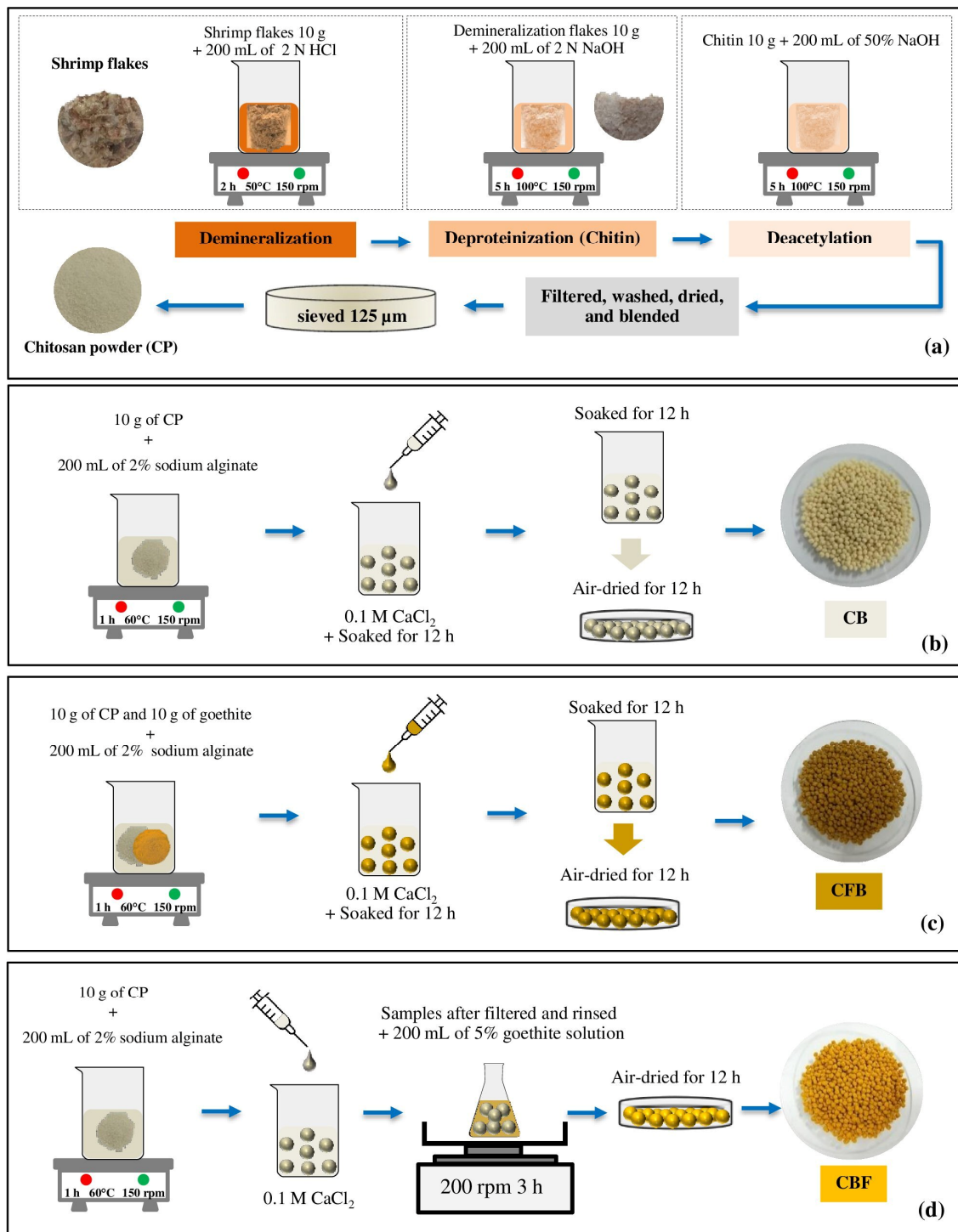


Figure 1. The chitosan material synthesis of (a) chitosan powder (CP), (b) chitosan powder beads (CB), (c) chitosan powder mixed with goethite beads (CFB), and (d) chitosan powder beads coated with goethite (CBF).

Shrimp shell wastes were collected from the Banglamphu market, Muang Khon Kaen, Khon Kaen, Thailand. They were washed with tap water several times to remove pieces of tissue and other impurities and then rinsed with distilled water (DW). Next, they were dried at 80 °C for 24 h in a hot air oven (FED 53, Binder, Bohemia, NY, USA), and they were ground to a flake. Finally, they were kept in a desiccator before use.

Step 2: Demineralization

First, 10 g of shrimp shell flake was added to 200 mL of 2 N HCl, and then it was mixed using a hot plate (C-MAG HS 7, IKA, Rawang, Malaysia) at 50 °C with a magnetic stirrer of 150 rpm for 2 h. Secondly, it was washed with tap water until obtaining a neutral pH. Thirdly, it was rinsed with distilled water and dried in a hot air oven at 40 °C. Finally, it was blended and kept in a desiccator until use, and was called the demineralized flake.

Step 3: Deproteinization

First, 10 g of demineralized flake from Step 1 was added to 200 mL of 2 N NaOH, and then it was mixed using a hot plate at 100 °C with a magnetic stirrer of 150 rpm for 5 h. Secondly, it was filtered and washed with tap water until obtaining a neutral pH. Thirdly, it was rinsed with distilled water and dried in a hot air oven at 40 °C. Finally, it was blended and kept in a desiccator until use, and was called chitin.

Step 4: Deacetylation

First, 10 g of chitin from Step 2 was added to 200 mL of 50% NaOH, and then it was mixed using a hot plate at 100 °C with a magnetic stirrer of 150 rpm for 5 h. Secondly, it was filtered and washed with tap water until obtaining a neutral pH. Thirdly, it was rinsed with distilled water and dried in a hot air oven at 40 °C. Then, chitosan flakes were blended and filtered through a sieve of 125 µm. Finally, it was kept in a desiccator before use and was called chitosan powder (CP).

2.3. The Synthesis of Three Chitosan Materials (CB, CFB, and CBF)

The synthesis of three chitosan materials which were chitosan powder beads (CB), chitosan powder mixed with goethite beads (CFB), and chitosan powder beads coated with goethite (CBF) was modified from Ngamsurach, P et al., 2022 [30] and is illustrated in Figure 1b–d.

For the CB, 10 g of CP was added to 200 mL of 2% NaC₆H₇O₆ solution, and a hot plate at 60 °C with a magnetic stirrer of 150 rpm was used for the mixing for 1 h. After that, they were contained in a 10 mL syringe and were added dropwise into 225 mL of 0.1 M CaCl₂ solution. After that, they were soaked in 0.1 M CaCl₂ solution for 12 h for setting the beads. Finally, they were filtered, and deionized water (DI water) was used for rinsing many times. After that, they were dried for 12 h and kept in desiccators until use.

For the CFB, 10 g of CP and 10 g of FeO(OH) were added to 200 mL of 2% NaC₆H₇O₆ solution, and a hot plate at 60 °C with a magnetic stirrer of 150 rpm was used for the mixing for 1 h. After that, they were contained in a 10 mL syringe and were added dropwise into 225 mL of 0.1 M CaCl₂ solution. After that, they were soaked in 0.1 M CaCl₂ solution for 12 h for setting the beads. Finally, they were filtered, and DI water was used for rinsing many times. After that, they were dried for 12 h and kept in desiccators until use.

For the CBF, 10 g of CP was added to 200 mL of a 2% NaC₆H₇O₆ solution, and they were homogeneously mixed using a hot plate at 60 °C with a magnetic stirrer of 150 rpm for 1 h. Then, they were contained in a 10 mL syringe and were added dropwise into 225 mL of 0.1 M CaCl₂ solution, were filtered, and DI water was used for rinsing many times. Then, the bead samples were added to 200 mL of 5% FeO(OH) solution and shaken for 3 h at room temperature via an orbital shaker (GFL, 3020, Germany) at 150 rpm. Finally, they were filtered, and DI water was used for rinsing many times. After that, they were dried for 12 h and kept in desiccators until use.

2.4. Material Characterizations

The specific surface area, pore volumes, and pore sizes of the chitosan powder beads (CB), chitosan powder mixed with goethite beads (CFB), and chitosan powder beads coated with goethite (CBF) were determined according to Brunauer–Emmett–Teller (BET) (QUADRASORB evo™, Austria) via isothermal nitrogen gas (N₂) adsorption–desorption at 77.3 K with a degas temperature of 80 °C for 6 h. An X-ray diffractometer (XRD) (Bruker, D8 Advance, Switzerland) in the range of 2θ = 5–80° was used to analyze the crystalline structures of the commercial chitosan standard (STD), chitosan powder (CP), CB, CFB, and

CBF. With the use of field emission scanning electron microscopy and a focus ion beam (FESEM-FIB) with an energy dispersive X-ray spectrometer (EDX) (FEI, Helios NanoLab G3 CX, USA), we investigated the surface morphologies and chemical compositions of the CB, CFB, and CBF. Finally, the chemical functional groups of STD, CP, CB, CFB, and CBF were identified via Fourier-transform infrared spectroscopy (FTIR) (Bruker, TENSOR27, Hong Kong) in a range of 4000–600 cm^{-1} .

2.5. Batch Adsorption Experiments

The lead removal efficiencies of chitosan powder beads (CB), chitosan powder mixed with goethite beads (CFB), and chitosan powder beads coated with goethite (CBF) were examined via a series of batch experiments for the affecting factors of dose, contact time, pH, and concentration. To compare their lead removal efficiencies in batch experiments, the effects of dose (0.1–0.5 g), contact time (0–24 h), pH (3, 5, 7, and 9), and concentration (25–125 mg/L) were investigated. The control conditions of the lead concentration of 50 mg/L, a sample volume of 200 mL, a temperature of 25 °C, and a shaking speed (New Brunswick™, Innova 42, USA) of 200 rpm were applied. An atomic absorption spectrophotometer (AAS) (PerkinElmer, PinAAcle 900 F, USA) was used to analyze the lead concentration in all samples. The optimum condition was chosen by the lowest value of each affecting factor whilst obtaining the highest lead removal efficiency, and that value was applied to the next affecting factor studies. The lead removal efficiency in the percentage was calculated using Equation (1).

$$\text{Lead removal efficiency (\%)} = (C_0 - C_e)/C_0 \times 100 \quad (1)$$

where C_0 and C_e (mg/L) are the initial and final lead concentrations in the solution (mg/L).

2.6. Adsorption Isotherms

Adsorption isotherms were used to investigate the concentration or quantity of the adsorbed solute via the weight of adsorbents for homogeneous or heterogeneous adsorbent surfaces on a monolayer or multilayer, which are generally analyzed using linear Langmuir and Freundlich isotherms following Equations (2) and (3):

$$\text{Langmuir isotherm: } C_e/q_e = 1/K_L q_{\max} + C_e/q_{\max} \quad (2)$$

$$\text{Freundlich isotherm: } \log q_e = \log K_F + 1/n (\log C_e) \quad (3)$$

where q_e is the equilibrium adsorption capacity (mg/g), q_{\max} is the maximum adsorption capacity (mg/g), K_L is the Langmuir constant (L/mg), C_e is the equilibrium residual adsorbate concentration (mg/L), K_F is the Freundlich constant (mg/g)(L/mg) $^{1/n}$, and $1/n$ is the measure of intensity.

For the adsorption isotherm experiments, 0.5 g of CB, 0.5 g of CFB, or 0.4 g of CBF were added to 500 mL Erlenmeyer flasks with a variable series of lead concentrations of 25, 50, 75, 100, and 125 mg/L. The control conditions were a sample volume of 200 mL, a contact time of 15 h for CB, 15 h for CFB, or 14 h for CBF, pH 5, a temperature of 25 °C, and a shaking speed of 150 rpm.

2.7. Adsorption Kinetics

Adsorption kinetics were used to explain the mechanisms of lead adsorption on chitosan bead materials. The adsorption characteristics of chitosan materials were demonstrated using the pseudo-first-order and pseudo-second-order kinetic equations following Equations (4) and (5).

$$\text{Pseudo-first-order kinetic model: } \ln(q_e - q_t) = \ln q_e - k_1 t \quad (4)$$

$$\text{Pseudo-second-order kinetic model : } t/q_t = t/q_e + 1/(k_2q_e^2) \quad (5)$$

where q_e is the equilibrium adsorption capacity (mg/g), q_t is the amount of the amount adsorbed at equilibrium at a time t (mg/g), k_1 is the pseudo-first-order rate constant (1/min), t is the time for adsorption (min), and k_2 is the pseudo-second-order rate constant per min (g/mg·min).

For the kinetic adsorption experiments, 0.5 g of CB, 0.5 g of CFB, or 0.4 g of CBF were added to 1000 mL of the breaker with a lead concentration of 50 mg/L. The control conditions were a sample volume of 200 mL, a contact time of 16 h for CB, 16 h for CFB, or 14 h for CBF, pH 5, a temperature of 25 °C, and a shaking speed of 150 rpm.

2.8. Desorption Experiments

The desorption experiments were used to verify the reusability of the chitosan materials. In adsorption, 0.5 g of chitosan powder beads (CB), 0.5 g of chitosan powder mixed with goethite beads (CFB), or 0.4 g of chitosan powder beads coated with goethite (CBF) were added to 500 mL Erlenmeyer flasks with a lead concentration of 50 mg/L. The control conditions were a sample volume of 200 mL, a contact time of 16 h for CB, 16 h for CFB, or 14 h for CBF, pH 5, a temperature of 25 °C, and a shaking speed of 150 rpm. In desorption, the saturated chitosan materials were rinsed several times with deionized water and added to 500 mL Erlenmeyer flasks with 0.5 M HNO₃. The control conditions were a sample volume of 100 mL, a contact time of 16 h for CB, 16 h for CFB, or 14 h for CBF, a temperature of 25 °C, and a shaking speed of 150 rpm. After that, they were washed with deionization water and dried at room temperature, and CB, CFB, and CBF were ready for the next adsorption cycle.

3. Results and Discussion

3.1. The Physical Characterizations

The physical characterizations of the commercial chitosan standard (STD), chitosan powder (CP), chitosan powder beads (CB), chitosan powder mixed with goethite beads (CFB), and chitosan powder beads coated with goethite (CBF) are shown in Figure 2a–e. CP was a cream-color powder matching the color of STD, as demonstrated in Figure 2a,b. For CB, they were cream-color beads similar to the color of CP, as illustrated in Figure 2c, whereas the CFB were dark-yellow-color beads, as shown in Figure 2d. Finally, the CBF were orange-yellow-color beads, as shown in Figure 2e.

3.2. Chitosan Material Characterizations

3.2.1. BET

BET analysis was used to identify the specific surface area, pore volume, and pore size of chitosan powder beads (CB), chitosan powder mixed with goethite beads (CFB), and chitosan powder beads coated with goethite (CBF). The results from the BJH method are demonstrated in Table 2, and their BJH pore size distribution is illustrated in Figure 3. The specific surface areas of the CB, CFB, and CBF were 1.453, 2.305, and 1.959 m²/g, respectively, whereby the CFB had the largest size of surface area. The pore volumes of the CB, CFB, and CBF were 0.0049, 0.0115, and 0.0054 cm³/g, respectively, and the CFB had the larger pore volume. The pore sizes of the CB, CFB, and CBF were 3.01, 1.80, and 1.81 nm, respectively, and the CFB had the smallest pore size. Therefore, the addition of goethite into the chitosan beads helped to increase the specific surface area and pore volume, promoting more active sites for capturing more lead [52], while the pore size was decreased, and these characteristics were good and similar to the lead adsorption reports from previous investigations [26,29,42,43,53]. Moreover, according to the International Union of Pure and Applied Chemistry (IUPAC) classification of pore size based on diameter, the CFB and CBF were micropores (2 nm), and the CB were mesopores (2–50 nm) [54].

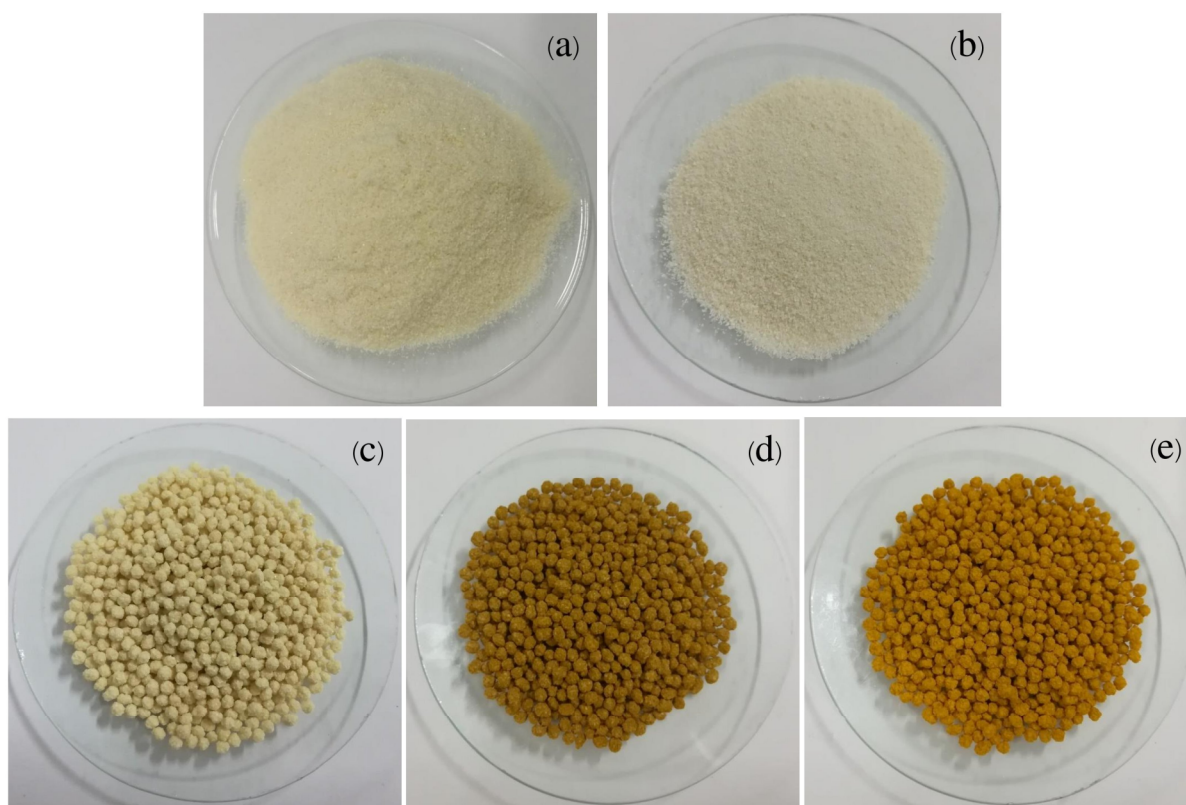


Figure 2. The physical characterizations of (a) commercial chitosan standard (STD), (b) chitosan powder (CP), (c) chitosan powder beads (CB), (d) chitosan powder mixed with goethite beads (CFB), and (e) chitosan powder beads coated with goethite (CBF).

Table 2. The specific surface area, pore volumes, and pore sizes of chitosan powder beads (CB), chitosan powder mixed with goethite beads (CFB), and chitosan powder beads coated with goethite (CBF).

Materials	Specific Surface Area (m ² /g)	Pore Volume (cm ³ /g)	Pore Size (nm)
CB	1.453	0.0049	3.01
CFB	2.305	0.0115	1.81
CBF	1.959	0.0054	1.80

3.2.2. XRD

The XRD technique was used to study the crystalline formations of commercial chitosan standard (STD), chitosan powder (CP), chitosan powder beads (CB), chitosan powder mixed with goethite beads (CFB), and chitosan powder beads coated with goethite (CBF), and their XRD patterns are described in Figure 4a–e. All materials were semicrystalline structures, and the diffraction patterns of the chitosan materials were changed by modifying the forms and adding goethite. The crystalline structure of CP matched the diffraction pattern of STD at 2θ of 20° representing the hydrogen bonds in the chitosan structure, shown in Figure 4a,b, similar to that found in other studies [30,55]. The CB had a lower crystalline structure than CP in a range of $2\theta = 20^\circ$, while the pattern at $2\theta = 13^\circ$ was more crystalline than CP and was demonstrated to contain sodium alginate, indicating that the crystalline structure of the chitosan material was altered by the bead forms shown in Figure 4b,c [56]. For the CFB and CBF, they represented more amorphous structures than the CB and demonstrated the goethite diffraction pattern at $2\theta = 21^\circ$, 33° , and 36° , shown in Figure 4d,e [57,58].

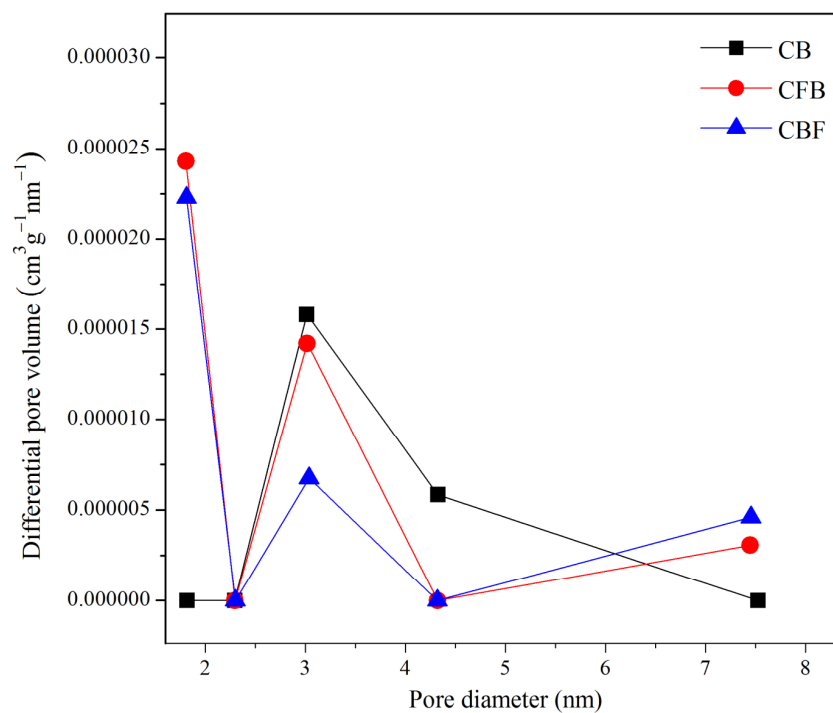


Figure 3. BJH pore size distribution of chitosan powder beads (CB), chitosan powder mixed with goethite beads (CFB), and chitosan powder beads coated with goethite (CBF).

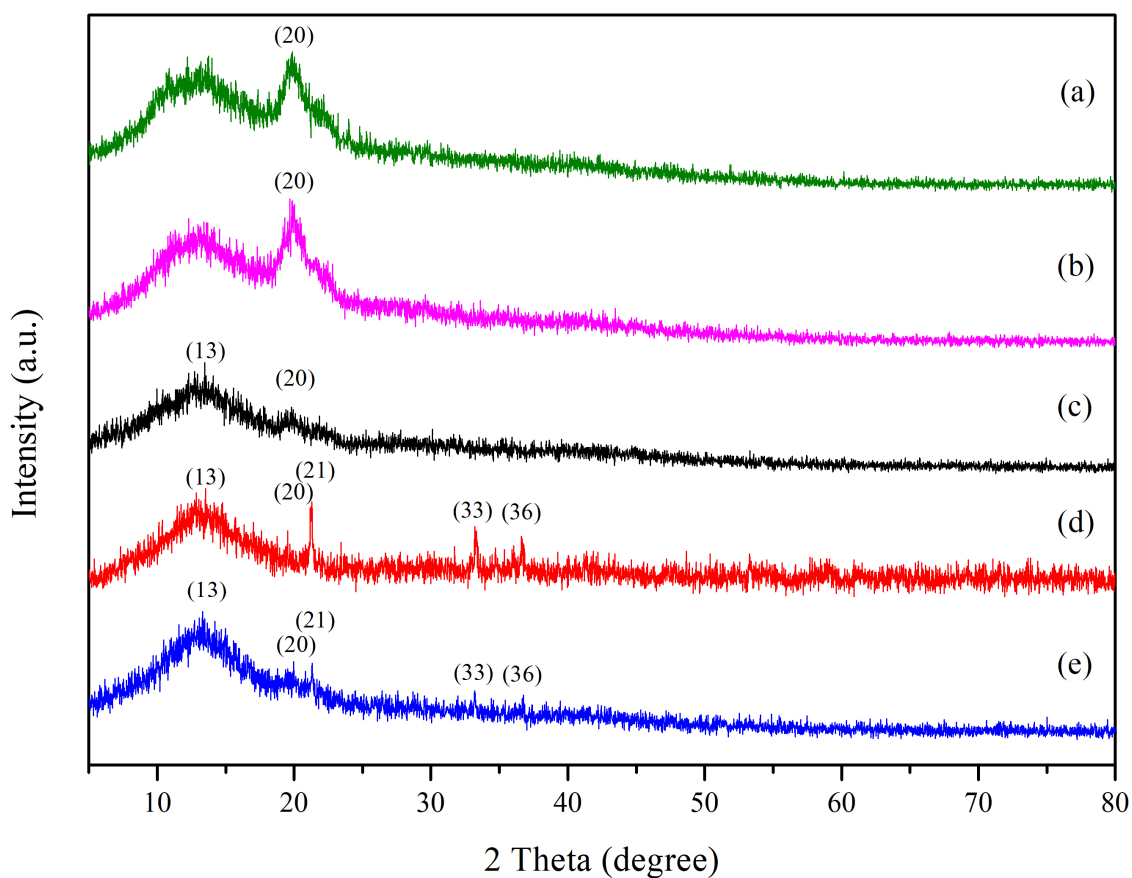


Figure 4. The XRD patterns of (a) commercial chitosan standard (STD), (b) chitosan powder (CP), (c) chitosan powder beads (CB), (d) chitosan powder mixed with goethite beads (CFB), and (e) chitosan powder beads coated with goethite (CBF).

3.2.3. FESEM-FIB

The surface structures of chitosan material chitosan powder beads (CB), chitosan powder mixed with goethite beads (CFB), and chitosan powder beads coated with goethite (CBF) were investigated using FESEM-FIB analysis at $2500\times$ magnification with $50\ \mu\text{m}$ for a surface structure and $100\times$ magnification with $1\ \text{mm}$ for a bead form, as shown in Figure 5a–f. The surface structures of chitosan materials were heterogeneous with spherical shapes. The CB were uneven, rough, and a little wavy, as shown in Figure 5a,b. Furthermore, because of the presence of a group of goethite mixed into the surface of the material, the surfaces of the CFB and CBF were rougher than the CB. In Figure 5c,d, the CFB were demonstrated as being lumpy and sparsely needle-shaped, while the CBF were presented with a surface with dense needle-shaped patterns, as shown in Figure 5e,f.

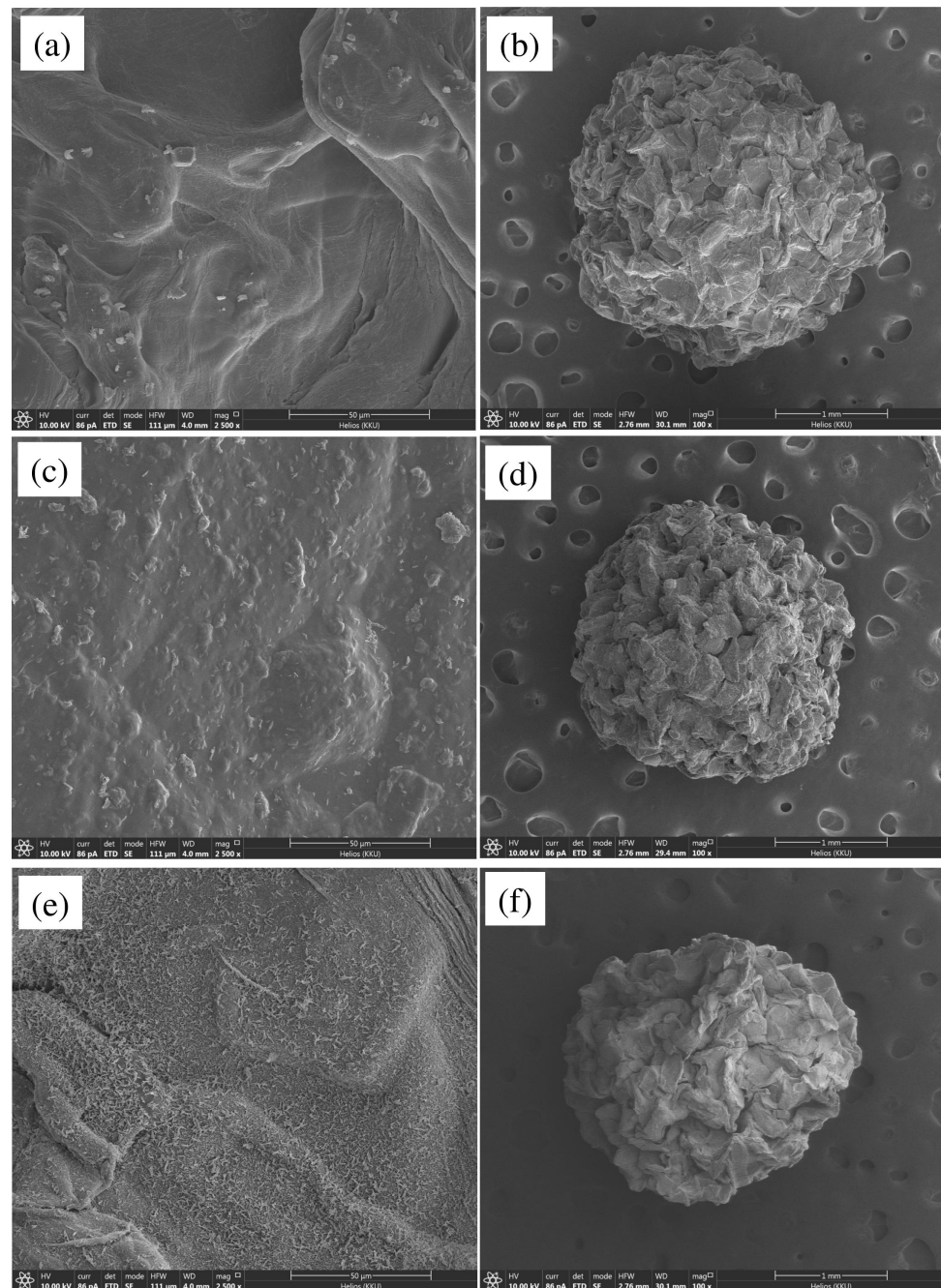


Figure 5. The surface structures of (a,b) chitosan powder beads (CB), (c,d) chitosan powder mixed with goethite beads (CFB), and (e,f) chitosan powder beads coated with goethite (CBF).

3.2.4. EDX

The chemical compositions of the chitosan material chitosan powder beads (CB), chitosan powder mixed with goethite beads (CFB), and chitosan powder beads coated with goethite (CBF) were analyzed using the EDX technique as demonstrated in Table 3. The six main chemical compositions of oxygen (O), carbon (C), calcium (Ca), nitrogen (N), chlorine (Cl), and sodium (Na) were detected in all chitosan materials, whereas the iron (Fe) was observed in only the CFB and CBF because of the addition of goethite. O, C, and N were the main chemical elements of the chitosan material from shrimp shells, as similarly found in previous studies [30,59]. For Ca, Cl, and Na, they were from the sodium alginate ($\text{NaC}_6\text{H}_7\text{O}_6$) and calcium chloride (CaCl_2) used for bead formation. In addition, the addition of goethite in CFB and CBF affected the mass percentages of the chemical compositions by decreasing O, C, Ca, N, Cl, and Na by the substitution of Fe, whereby the addition of goethite via the coating method of the CBF found a higher percentage by weight of Fe than the mixing method of the CFB. As a result, the CBF had a higher decrease in all chemical compositions than the CFB, except for Na.

Table 3. Chemical compositions of chitosan bead materials with percentages by weight.

Materials	Chemical Compositions (% wt.)						
	O	C	Ca	N	Cl	Na	Fe
CB	45.4	38.7	5.8	5.2	4.1	0.8	0
CFB	44.8	35.5	5.2	4.8	2.7	0.2	6.8
CBF	39.4	30.7	1.9	4.5	0.3	0.2	23.0

3.2.5. FTIR

The functional groups of commercial chitosan standard (STD), chitosan powder (CP), chitosan powder beads (CB), chitosan powder mixed with goethite beads (CFB), and chitosan powder beads coated with goethite (CBF) were investigated using FTIR spectra, as shown in Figure 6a–e. Five main function groups of N–H, O–H, C–H, C–O, and –COOH were detected in all of the materials. O–H referred to the stretching of the hydroxyl group and –NH₂ represented the stretching of amines. C–H presented the methyl group (–CH₂) in the CH₂OH group and C–O was the stretching of the alcoholic group, as similarly found in previous studies [49,60–62]. Furthermore, the N–H bending, overlapping, stretching, strong vibrations of –COOH in the carboxylate represented sodium alginate in the CB, CFB, and CBF. The overlapping confirms the formation of electrostatic interactions between amines (–NH₂) and carboxylic groups (–COOH) in chitosan bead form [63,64]. Moreover, the strong absorption peaks at 700–900 cm^{−1} were caused by the bending vibration of the surface hydroxyl (O–H) of Fe–O–OH in goethite, indicating that goethite was involved in the CFBs' and CBFs' structures, similar to those reported in the literature [58,65]. Regarding CP, it presented similar functional groups with STD, illustrating the –NH₂ and O–H detected at 3359 cm^{−1}, C–H at 2873 cm^{−1} and 1422 cm^{−1}, N–H at 1589 cm^{−1}, and C–O at 1025 cm^{−1}, as shown in Figure 6a,b. For the CB, we observed –NH₂ and O–H detected at 3344 cm^{−1}, C–H at 1417 cm^{−1}, the bending overlapping of –COOH and N–H at 1592 cm^{−1}, and C–O at 1024 cm^{−1}, as shown in Figure 6c. For the CFB, we found –NH₂ and O–H detected at 3106 cm^{−1}, C–H at 1416 cm^{−1}, the bending overlapping of –COOH and N–H at 1593 cm^{−1}, C–O at 1026 cm^{−1}, and Fe–O–OH (O–H) at 897 cm^{−1}, as shown in Figure 6d. Finally, the CBF were identified to have –NH₂ and O–H detected at 3283 cm^{−1}, C–H at 1416 cm^{−1}, the bending overlapping of –COOH and N–H at 1591 cm^{−1}, C–O at 1025 cm^{−1}, and Fe–O–OH (O–H) at 798 cm^{−1}, as shown in Figure 6e.

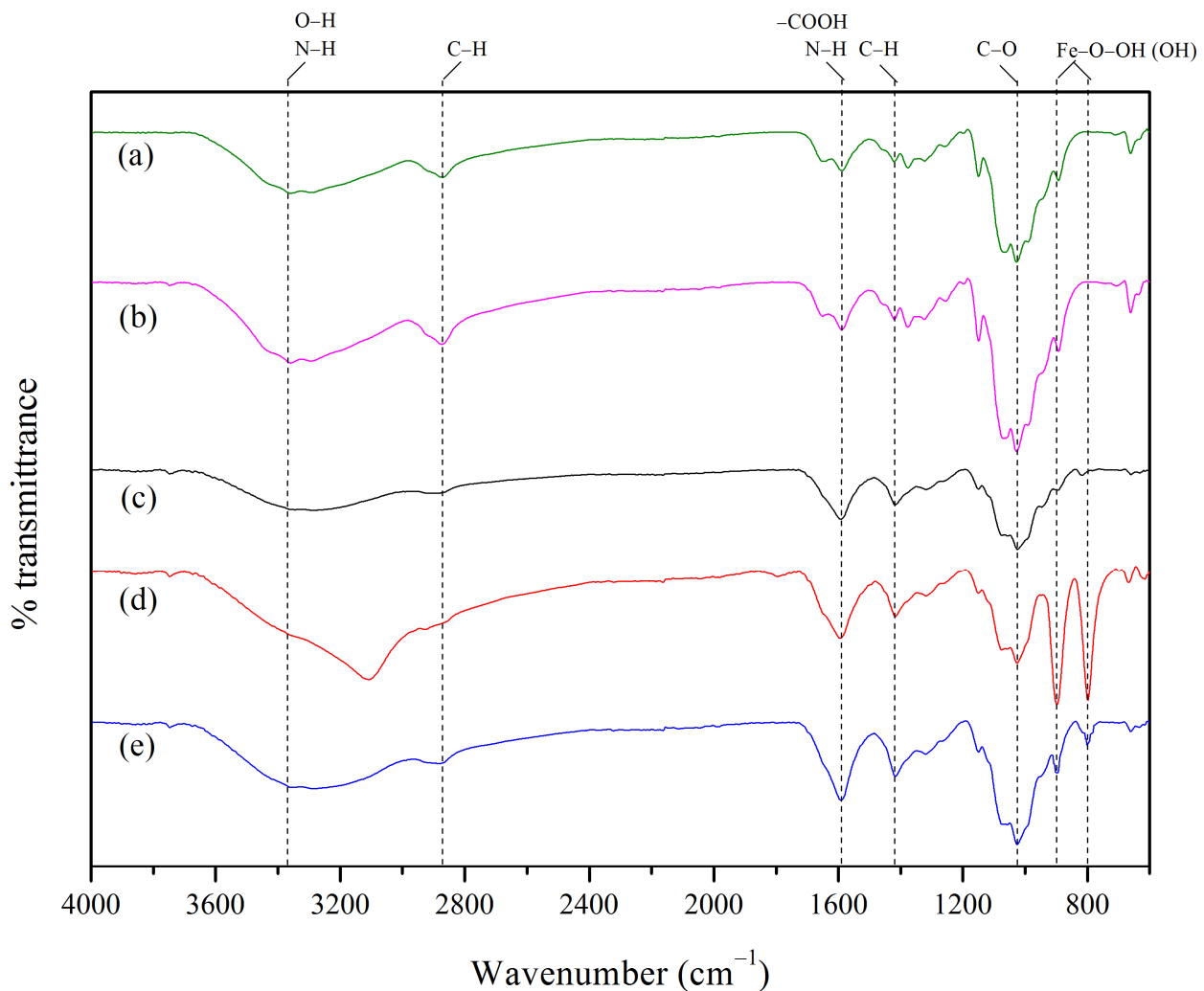


Figure 6. FTIR spectra of (a) commercial chitosan standard (STD), (b) chitosan powder (CP), (c) chitosan powder beads (CB), (d) chitosan powder mixed with goethite beads (CFB), and (e) chitosan powder beads coated with goethite (CBF).

3.3. Batch Experiments

3.3.1. Effect of Dose

Chitosan powder beads (CB), chitosan powder mixed with goethite beads (CFB), and chitosan powder beads coated with goethite (CBF) were investigated for the effect of dose from 0.1 to 0.5 g, as shown in Figure 7a, with a lead concentration of 50 mg/L, a sample volume of 200 mL, a contact time of 24 h, a shaking speed of 150 rpm, and a temperature of 25 °C as the control conditions. The lead removal efficiencies of the CB, CFB, and CBF increased with increasing dosages because of the increase in the material active sites [30], and the highest lead removal efficiencies of the CB and CFB were found at 0.5 g for 99.14% and 99.32%, respectively. For the CBF, the highest lead removal efficiency of 99.57% was found at 0.4 g. Therefore, the optimum dosages of the CB, CFB, and CBF were 0.5 g, 0.5 g, and 0.4 g, respectively, and were used for the contact time effect.

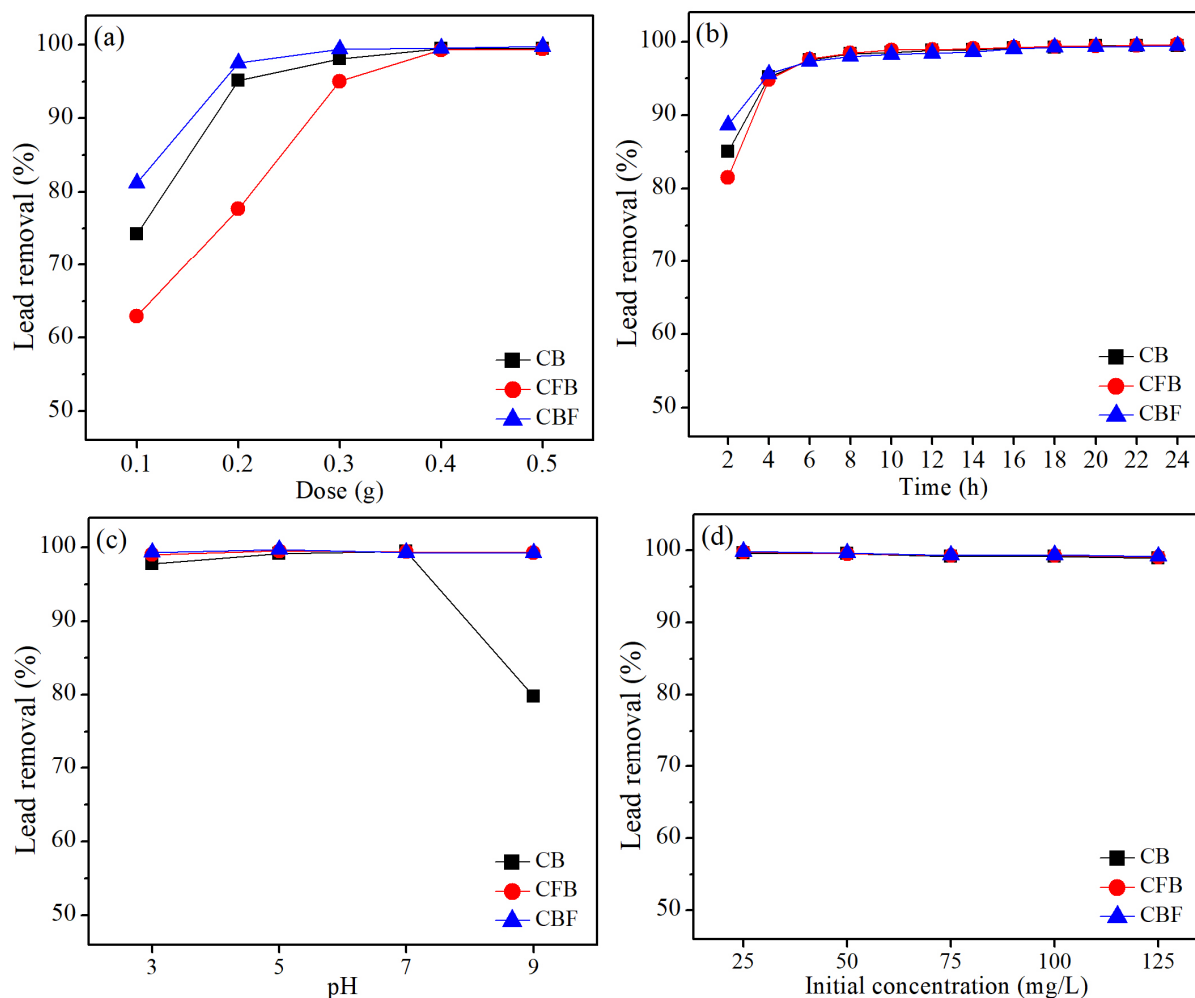


Figure 7. The effects of (a) dose, (b) contact time, (c) pH, and (d) initial lead concentrations according to a series of batch experiments on chitosan powder beads (CB), chitosan powder mixed with goethite beads (CFB), and chitosan powder beads coated with goethite (CBF).

3.3.2. Effect of Contact Time

Chitosan powder beads (CB), chitosan powder mixed with goethite beads (CFB), and chitosan powder beads coated with goethite (CBF) had their contact time effect studied from 2 to 24 h, shown in Figure 7b, with a lead concentration of 50 mg/L, a sample volume of 200 mL, a shaking speed of 150 rpm, a temperature of 25 °C, and the optimum dose from Section 3.3.1 as the control conditions. The lead removal efficiencies of the CB, CFB, and CBF increased with increasing contact time from 2 to 24 h, and their saturated lead adsorptions were found at the highest contact time with the constant lead removal efficiency. The highest lead removal efficiencies of 99.09%, 99.25%, and 99.62% were found at 16 h for CB and CFB, whereas for CBF it was found at 14 h, respectively. Therefore, the optimum contact time of the CB, CFB, and CBF was 16 h, 16 h, and 14 h, respectively, and was used for the pH effect.

3.3.3. Effect of pH

Chitosan powder beads (CB), chitosan powder mixed with goethite beads (CFB), and chitosan powder beads coated with goethite (CBF) were examined for their pH effects of 3, 5, 7, and 9, shown in Figure 7c, with a sample volume of 200 mL, a shaking speed of 150 rpm, a temperature of 25 °C, and the optimum dose and contact time from Section 3.3.1 and Section 3.3.2 as the control conditions. The lead removal efficiencies at pH 3 of the CB, CFB, and CBF were 97.75%, 99.01%, and 99.30%, respectively. At a low pH, the active sites

of the chitosan materials were protonated, and the competition with proton (H^+) between the solution and the cation of lead might be the limit for lead removal [66]. Furthermore, many previous studies have reported that the point of zero charge (pH_{pzc}) of chitosan material was $pH > 4$ [46,63,67,68], and so lead removal might happen at a pH of solution more than pH_{pzc} ($pH > 4$). At pH 5, the lead removal efficiencies of the CB, CFB, and CBF increased to 99.41%, 99.49%, and 99.68%, respectively, which were the highest lead removal efficiencies in the entire pH range studied. At pH 7, the lead removal efficiencies of the CB, CFB, and CBF slightly decreased to 99.11%, 99.39%, and 99.28%, respectively. At pH 9, the lead removal efficiencies of the CB, CFB, and CBF decreased to 79.79%, 99.25%, and 99.24%, respectively.

The lead speciation diagram in the aqueous system is displayed in Figure 8, modified from Nurchi, V.M. and Villaescus, I. 2011 and Wang X. et al. 2017 [69,70]. In pH 4–6, lead could be adsorbed by the chitosan materials because of its status of $Pb(II)$ ions (aq). At $pH > 7$, the lead removal efficiencies might be limited due to an increase in hydroxyl products such as $Pb(OH)^+$, which is possible to remove via adsorption. However, lead precipitations might occur at $pH > 9$ becoming an insoluble $Pb(OH)_2(s)$ product, and lead adsorption might not happen from the observation found in CB [69,70]. In the case of the addition of goethite in the CFB and CBF, lead adsorptions could occur at all pH values with high lead removal efficiencies, which might be from the high pH_{pzc} of goethite ($pH > 8$) reported by previous studies [71–73]; so, the addition of goethite to the CFB and CBF improved the material efficiency for adsorbing lead in a wider pH range. Therefore, the optimum pH value of the CB, CFB, and CBF was pH 5 and was used for the initial lead concentration effect.

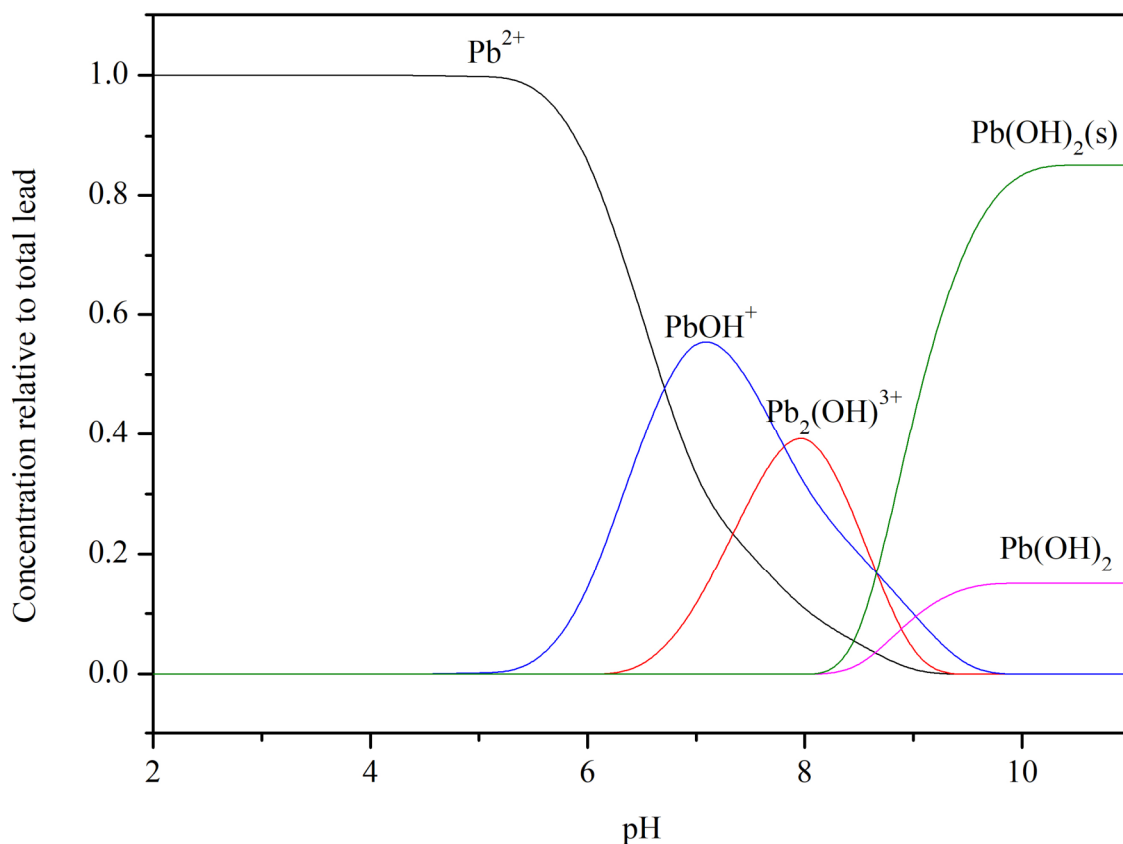


Figure 8. Effect of pH on lead speciation in aqueous systems at concentration of 50 mg/L.

3.3.4. Effect of Concentration

Chitosan powder beads (CB), chitosan powder mixed with goethite beads (CFB), and chitosan powder beads coated with goethite (CBF) were investigated for their initial

lead concentration effect from 50 mg/L to 125 mg/L, as shown in Figure 7d, with a sample volume of 200 mL, a shaking speed of 150 rpm, a temperature of 25 °C, and the optimum dose, contact time, and pH from Sections 3.3.1–3.3.3 as the control conditions. The lead removal efficiencies of the CB, CFB, and CBF did not affect the increasing lead concentrations, and they could remove lead from 25–125 mg/L with high lead removal efficiencies of more than 98%. However, their lead removal efficiencies at 50 mg/L were 99.27%, 99.52%, and 99.66%, respectively. Therefore, the CBF were a higher potential material than the CB and CFB.

Finally, 0.5 g, 16 h, pH 5, 50 mg/L, 0.5 g, 16 h, pH 5, 50 mg/L, and 0.4 g, 14 h, pH 5, 50 mg/L were the optimum conditions for dose, contact time, pH, and concentration of the CB, CFB, and CBF, respectively, and they could be arranged in order from high to low of CBF > CFB > CB. The CBF had a higher potential material than the CB and CFB because they required less material dosage and contact time.

3.4. Adsorption Isotherms

The adsorption isotherms of chitosan powder beads (CB), chitosan powder mixed with goethite beads (CFB), and chitosan powder beads coated with goethite (CBF) were observed by plotting linear Langmuir (C_e/q_e vs. C_e) and linear Freundlich ($\log q_e$ vs. $\log C_e$) models, whereby their plotted graphs are presented in Figures 9a,b and 10, and the equilibrium of linear isotherm parameters are reported in Table 4.

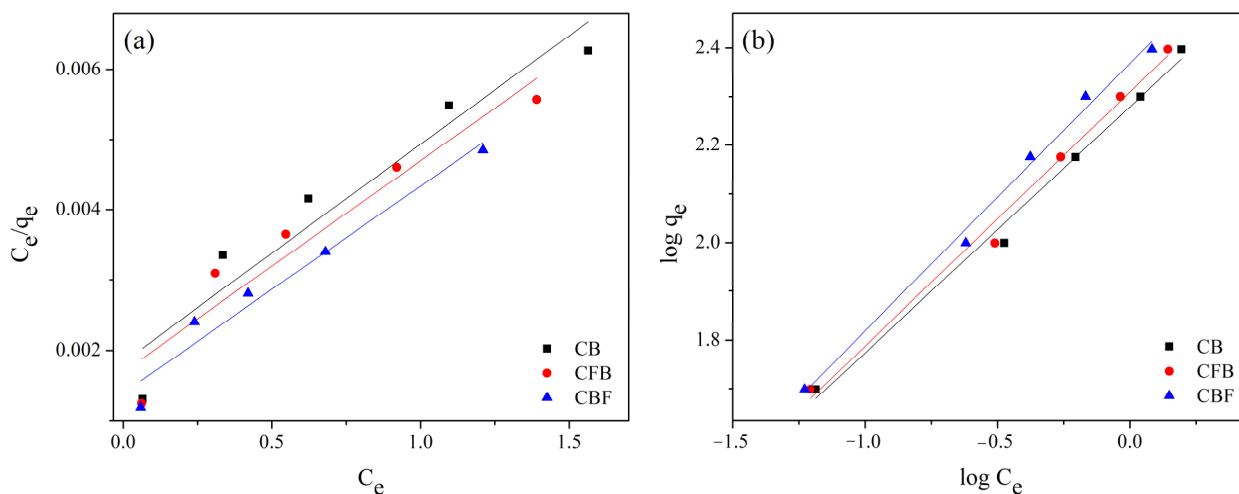


Figure 9. The adsorption isotherms of chitosan powder beads (CB), chitosan powder mixed with goethite beads (CFB), and chitosan powder beads coated with goethite (CBF) for (a) linear Langmuir model and (b) linear Freundlich model.

Table 4. The equilibrium of linear isotherm parameters of chitosan powder beads (CB), chitosan powder mixed with goethite beads (CFB), and chitosan powder beads coated with goethite (CBF) for lead adsorption.

Isotherm Models	Parameters	CB	CFB	CBF
Langmuir model	q_{\max} (mg/g)	322.58	333.33	344.83
	K_L (L/mg)	1.72	1.76	2.07
	R^2	0.923	0.922	0.961
Freundlich model	K_F (mg/g)(L/mg) $^{1/n}$	190.15	204	233.29
	$1/n$	0.51	0.52	0.55
	R^2	0.992	0.992	0.994

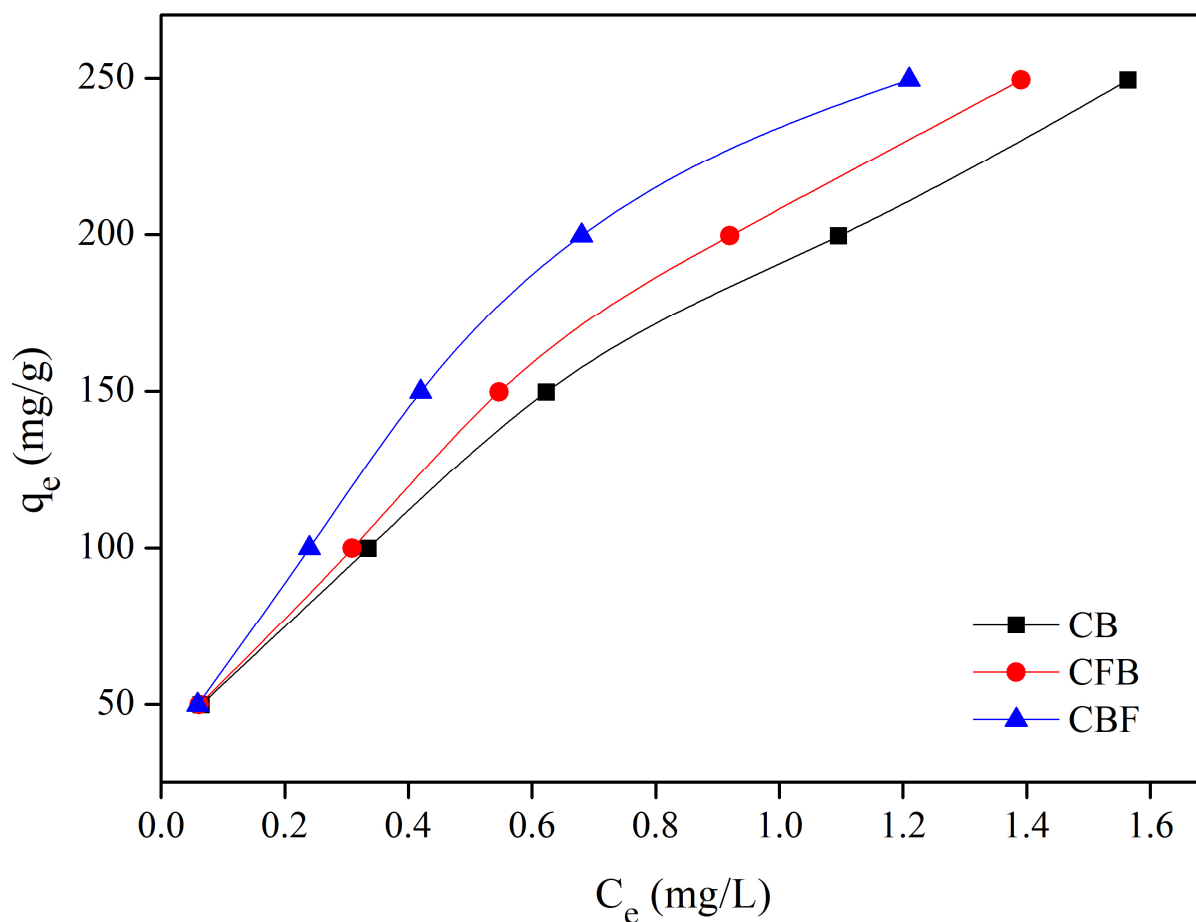


Figure 10. The adsorption isotherm of adsorption capacity (q_e) vs. lead concentration (C_e).

For the Langmuir model, the maximum adsorption capacities (q_{max}) of the CB, CFB, and CBF were 322.58, 333.33, and 344.83 mg/g, respectively, whereby the maximum adsorption capacity (q_{max}) of the CBF was demonstrated to be higher than the other materials. The Langmuir adsorption constants (K_L) of the CB, CFB, and CBF were 1.72, 1.76, and 2.07 L/mg, respectively. For the Freundlich model, the measure of intensity or the adsorption strength ($1/n$) values of the CB, CFB, and CBF were 0.51, 0.52, and 0.55, respectively, whereby the measure of intensity ($1/n$) of the CBF had a higher value than the other materials. The Freundlich adsorption constants (K_F) of the CB, CFB, and CBF were 190.15, 204, and 233.29 (mg/g)(L/mg) $^{1/n}$, respectively, whereby the K_F of the CBF demonstrated a higher value than the other materials. In general, the explanation of the adsorption pattern of each adsorption material is decided by the R^2 value of the adsorption isotherm model. Therefore, they are chosen with the correlation coefficient (R^2) value being especially close to 1. Finally, the CB, CFB, and CBF corresponded to the Freundlich model with an R^2 of 0.992, 0.992, and 0.994, respectively, which agrees with other studies [68,74–76]. As a result, the adsorption patterns of the CB, CFB, and CBF were explained by the physiochemical process, which was presented to the heterogeneous surfaces of all of the materials. Figure 10 demonstrated that the adsorption capacities (q_e) increased with the increase in lead concentrations in all materials, and their q_e could be arranged from high to low with CBF > CFB > CB.

3.5. Adsorption Kinetics

The adsorption kinetic is used to study the rate of adsorption over time of chitosan material chitosan powder beads (CB), chitosan powder mixed with goethite beads (CFB), and chitosan powder beads coated with goethite (CBF). Their rate adsorptions of lead

with chitosan materials were investigated using adsorption kinetic models which were pseudo-first-order and pseudo-second-order kinetic models, by plotting $\ln(q_e - q_t)$ versus time (t) for pseudo-first-order and t/q_t versus time (t) for pseudo-second-order, whereby their plotted graphs are demonstrated in Figure 11a,b, and their equilibrium of kinetic parameters is presented in Table 5.

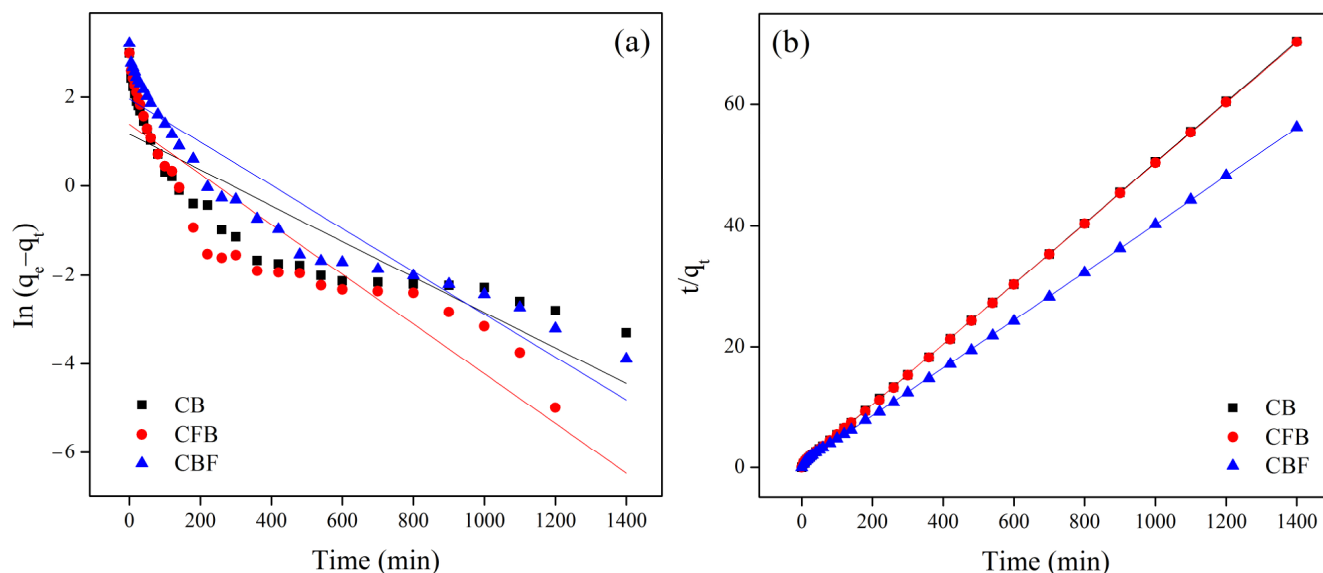


Figure 11. The adsorption kinetics of the chitosan powder beads (CB), chitosan powder mixed with goethite beads (CFB), and chitosan powder beads coated with goethite (CBF) on (a) linear pseudo-first-order kinetic model and (b) linear pseudo-second-order kinetic model.

Table 5. The equilibrium of kinetic parameters of chitosan powder beads (CB), chitosan powder mixed with goethite beads (CFB), and chitosan powder beads coated with goethite (CBF) for lead adsorptions.

Kinetic Models	Parameters	CB	CFB	CBF
Pseudo-first-order kinetic model	k_1 (1/min)	0.004	0.0056	0.0048
	q_e (mg/g)	3.20	4.01	7.05
	R^2	0.7729	0.8621	0.8894
Pseudo-second-order kinetic model	k_2 (g/mg·min)	0.0061	0.0052	0.0025
	q_e (mg/g)	20.00	20.10	25.25
	R^2	0.9997	0.9999	0.9999

The results demonstrated that the correlation coefficients (R^2) from the adsorption kinetic models of the CB, CFB, and CBF corresponded to the pseudo-second-order kinetic model at 0.9997, 0.9999, and 0.9999, respectively, as similarly reported by other studies [40,47,55,67], whereby the adsorption mechanism and the rate-determining step were the chemisorption mechanisms on the surface of all of the materials [77]. Furthermore, Figure 12 demonstrates that the rate of lead adsorption of chitosan bead materials achieved the equilibrium state within 200 min, whereby the CBF represented the highest adsorption capacity (q_e) at 25.25 mg/g, followed by the CFB at 20.10 mg/g and CB at 20.00 mg/g, respectively.

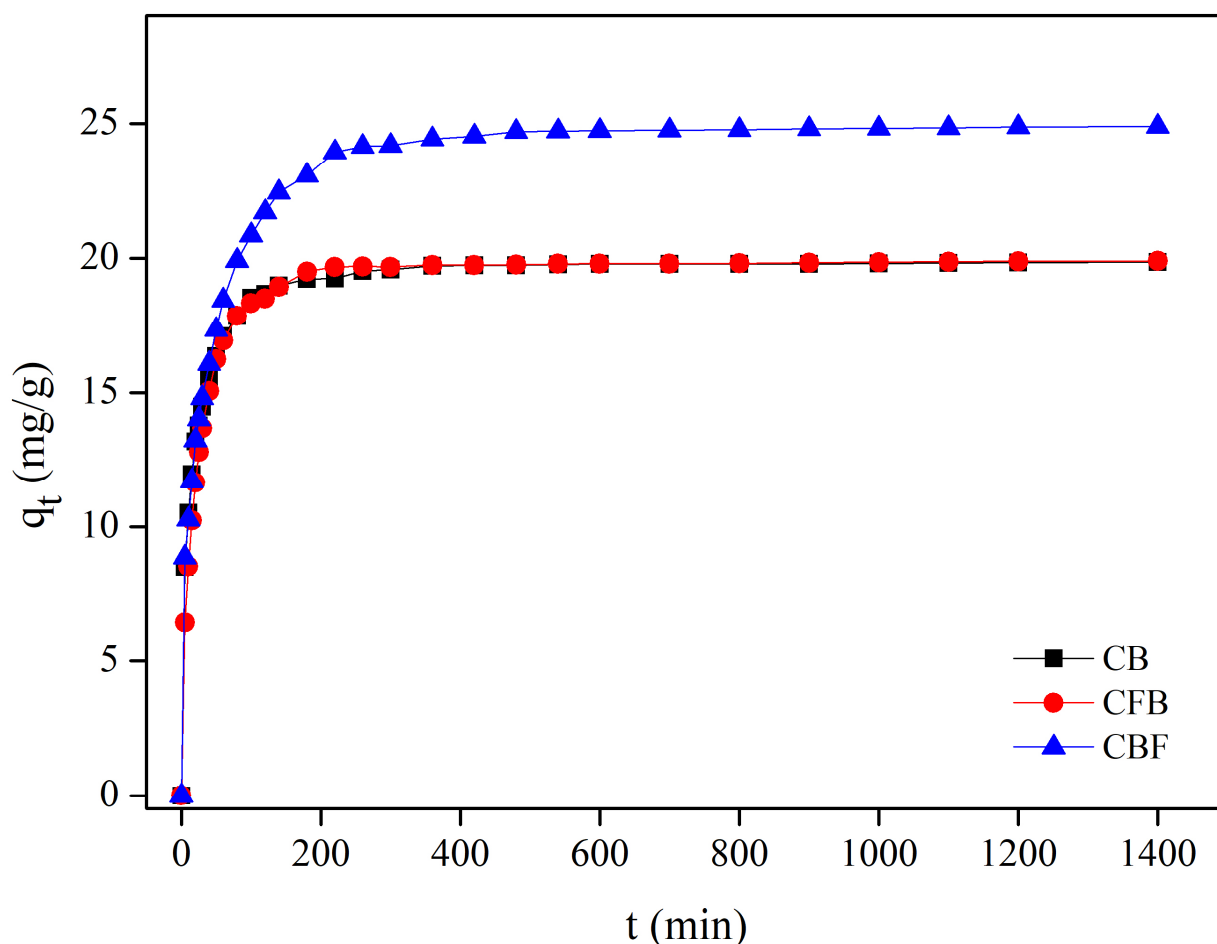


Figure 12. The adsorption equilibriums of chitosan powder beads (CB), chitosan powder mixed with goethite beads (CFB), and chitosan powder beads coated with goethite (CBF) for lead adsorptions.

3.6. Desorption Experiments

The adsorption and desorption experiments of chitosan powder beads (CB), chitosan powder mixed with goethite beads (CFB), and chitosan powder beads coated with goethite (CBF) for lead adsorption were investigated in three cycles using 0.1 M HNO_3 as the desorption eluent, and the results of the lead removal efficiency decreased gradually as the number of cycles increased, which is demonstrated in Figure 13.

For the CB, the lead adsorption efficiencies of three cycles were 99.49%, 97.71%, and 93.56%, respectively, while the lead desorption efficiencies of three cycles were 82.64%, 80.27%, and 75.32%, respectively. For the CFB, the lead adsorption efficiencies of three cycles were 99.60%, 97.89%, and 93.70%, respectively, while the lead desorption efficiencies of three cycles were 83.22%, 81.62%, and 73.70%, respectively. For the CBF, the lead removal efficiencies of three cycles were 99.62%, 97.88%, and 93.60%, respectively, while the lead desorption efficiencies of three cycles were 82.33%, 78.94%, and 75.21%, respectively. Moreover, their lead adsorption and desorption efficiencies after use in three cycles decreased by approximately 5.95% and 7.99%, respectively. As a result, they could be reused in more than three cycles with lead adsorptions of more than 73%.

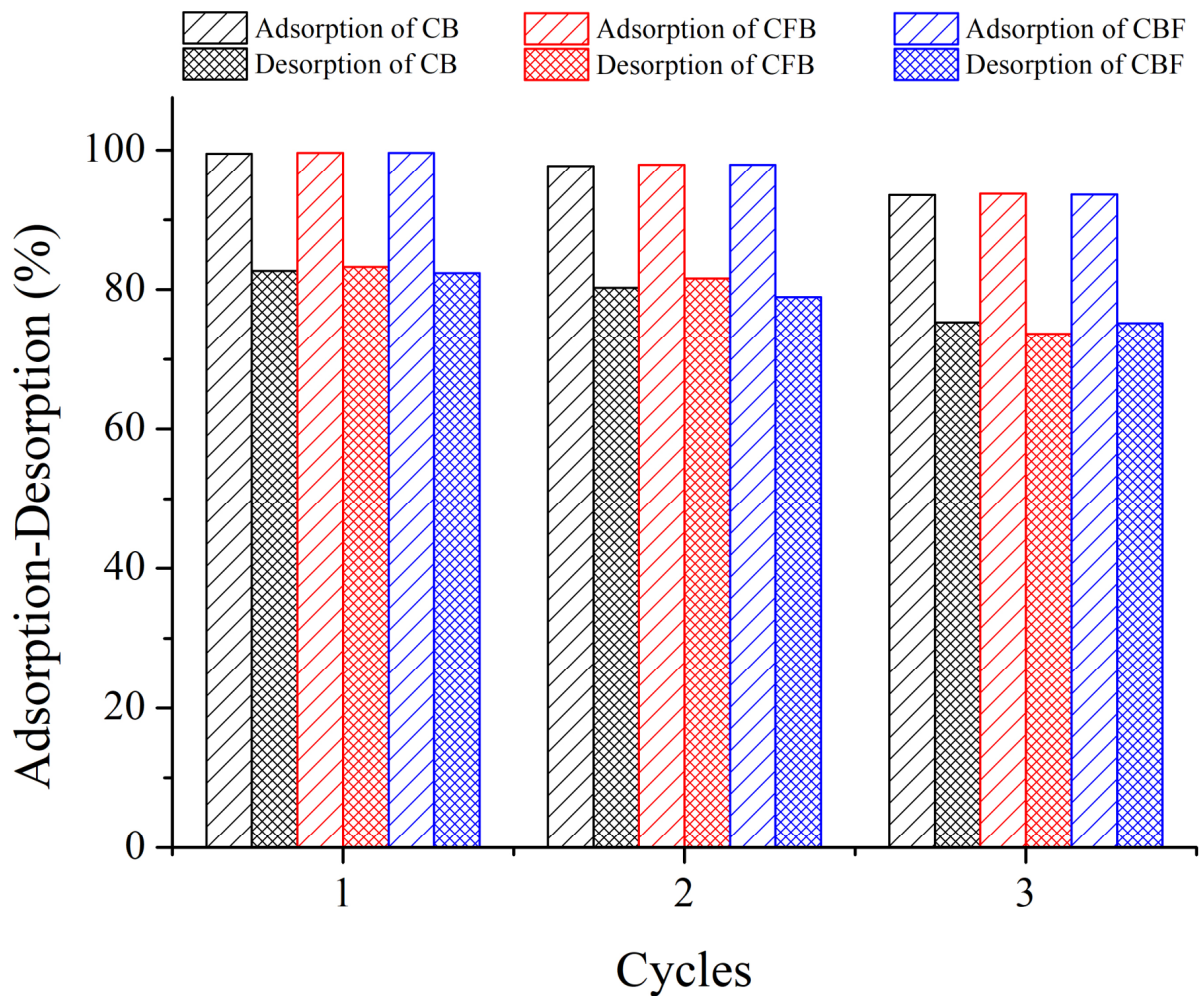


Figure 13. Lead adsorption and desorption of chitosan powder beads (CB), chitosan powder mixed with goethite beads (CFB), and chitosan powder beads coated with goethite (CBF) in three cycles.

3.7. Possibility of Mechanisms via Lead Adsorption for Chitosan Materials

The lead removal processes of chitosan powder beads (CB), chitosan powder mixed with goethite beads (CFB), and chitosan powder beads coated with goethite (CBF) are influenced by their chemical functional groups which consist of an amine group ($-\text{NH}_2$ or N-H), a hydroxyl group ($-\text{OH}$), and a carboxyl group ($-\text{COOH}$). Moreover, the CFB and CBF also had the chemical functional group of goethite ($\text{FeO}(\text{OH})$), which affected the capture of lead. The possible mechanisms for the lead adsorption of chitosan materials are demonstrated in Figure 14a–c, which modified the idea from the study of Ngamsurach, P et al. [30]. For CB, lead (II) ions (Pb^{2+}) will be adsorbed by the donating proton (H^+) of $-\text{NH}_2$, $-\text{OH}$, and $-\text{COOH}$ followed by Pb^{2+} replacement via electrostatic interaction [60,62,63,65,78,79], as shown in Figure 14a. For CFB and CBF, lead adsorption might happen similarly to CB. In addition, lead adsorption might be from the chitosan materials and sodium alginate connected with $\text{FeO}(\text{OH})$ by covalent and hydrogen bonds [58,80], as illustrated in Figure 14b,c.

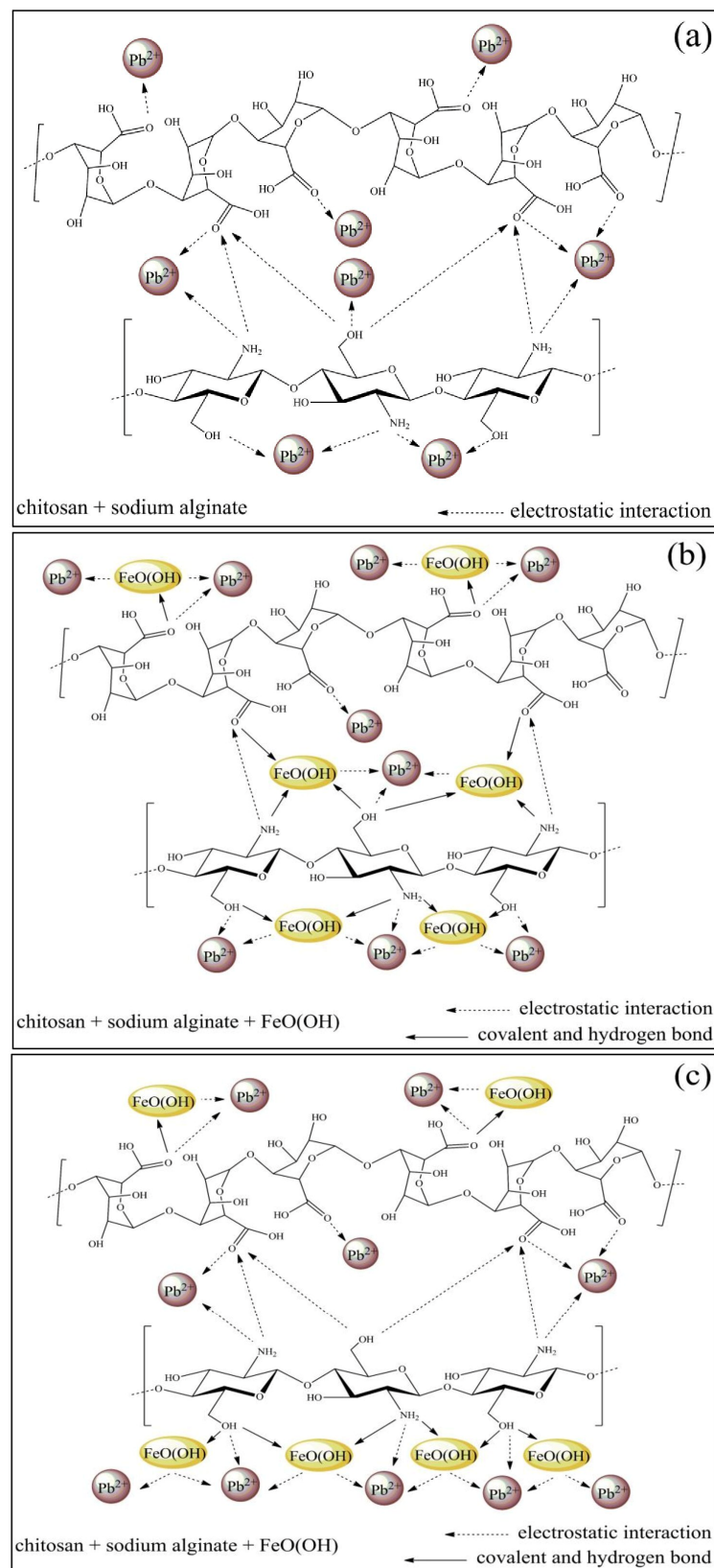


Figure 14. The possible mechanisms of lead adsorption of (a) chitosan powder beads (CB), (b) chitosan powder mixed with goethite beads (CFB), and (c) chitosan powder beads coated with goethite (CBF).

4. Conclusions

Shrimp shell wastes were successfully extracted to chitosan powder (CP) and were synthesized to the chitosan bead materials modified with or without goethite which were chitosan powder beads (CB), chitosan powder mixed with goethite beads (CFB), and chitosan powder beads coated with goethite (CBF) for lead removal in aqueous solution. They were semicrystalline structures, and the CFB and CBF were also found in the specific goethite peaks. The CBF illustrated the highest surface area and the smallest pore size compared to the CB and CFB. In addition, the pore sizes of the CFB and CBF were micropores, whereas those of the CB were mesopores. They had a spherical shape with heterogeneous surfaces. O, C, Ca, N, Cl, and Na were the main chemical components in all of the materials, and Fe was detected in the CFB and CBF due to the addition of goethite. N–H, O–H, C–H, C–O, and –COOH were the five main functional groups of all materials. For batch experiments, the lead removal efficiencies of all of the chitosan materials were more than 98% as seen via the optimum conditions of the CB, CFB, and CBF for lead removal efficiencies being 0.5 g, 16 h, pH 5, 0.5 g, 16 h, pH 5, and 0.4 g, 14 h, pH 5, respectively, indicating that the addition of goethite to chitosan materials improved their lead removal efficiencies. Moreover, all of the chitosan materials corresponded to the Freundlich model, which indicates the physiochemical process of their adsorption patterns. For adsorption kinetics, all of the chitosan materials corresponded to a pseudo-second-order kinetic model which was the chemisorption mechanism. The CBF demonstrated the highest lead adsorption capacity of 344.83 mg/g. The CB, CFB, and CBF could be reused for more than three cycles, with lead removal efficiencies above 90%. For future work, continuous flow experiments for investigating chitosan materials' efficiencies for applying wastewater treatment plants and the competing ion studies such as Mg^{2+} and Ca^{2+} should be studied to determine whether the chitosan bead materials could specifically adsorb lead in the solution.

Author Contributions: T.S.: investigation, visualization, writing—original draft. P.P.: supervision, conceptualization, funding acquisition, investigation, methodology, validation, formal analysis, visualization, writing—original draft, writing—review and editing. All authors have read and agreed to the published version of the manuscript.

Funding: This work has been financial supported by the research capability enhancement program through the graduate student scholarship, Faculty of Science, Khon Kaen University.

Data Availability Statement: The data presented in the study are available upon request from the corresponding author.

Conflicts of Interest: The authors declare that they have no known competing financial interests or personal relationships that could have appeared to influence the work reported in this paper.

References

1. Briffa, J.; Sinagra, E.; Blundell, R. Heavy metal pollution in the environment and their toxicological effects on humans. *Heliyon* **2020**, *6*, e04691. [[CrossRef](#)]
2. Liu, W.H.; Zhao, J.Z.; Ouyang, Z.Y.; Söderlund, L.; Liu, G.H. Impacts of sewage irrigation on heavy metal distribution and contamination in Beijing, China. *Environ. Int.* **2005**, *31*, 805–812. [[CrossRef](#)]
3. World Health Organization. *WHO Guideline for Clinical Management of Exposure to Lead*; WHO: Geneva, Switzerland, 2021.
4. Chowdhury, S.; Mazumder, M.A.J.; Al-Attas, O.; Husain, T. Heavy metals in drinking water: Occurrences, implications, and future needs in developing countries. *Sci. Total Environ.* **2016**, *569–570*, 476–488. [[CrossRef](#)] [[PubMed](#)]
5. Dedeke, G.A.; Iwuchukwu, P.O.; Aladesida, A.A.; Afolabi, T.A.; Ayanda, I.O. Impact of heavy metal bioaccumulation on antioxidant activities and DNA profile in two earthworm species and freshwater prawn from Ogun River. *Sci. Total Environ.* **2018**, *624*, 576–585. [[CrossRef](#)]
6. Rana, M.N.; Tangpong, J.; Rahman, M.M. Toxicodynamics of Lead, Cadmium, Mercury and Arsenic- induced kidney toxicity and treatment strategy: A mini review. *Toxicol. Rep.* **2018**, *5*, 704–713. [[CrossRef](#)]
7. Abdulla, M. Lead. In *Essential and Toxic Trace Elements and Vitamins in Human Health*; Elsevier: Amsterdam, The Netherlands, 2020; pp. 181–191. [[CrossRef](#)]
8. Ekramul Mahmud, H.N.M.; Obidul Huq, A.K.; Yahya, R.B. The removal of heavy metal ions from wastewater/aqueous solution using polypyrrole-based adsorbents: A review. *RSC Adv.* **2016**, *6*, 14778–14791. [[CrossRef](#)]

9. Carolin, C.F.; Kumar, P.S.; Saravanan, A.; Joshiba, G.J.; Naushad, M. Efficient techniques for the removal of toxic heavy metals from aquatic environment: A review. *J. Environ. Chem. Eng.* **2017**, *5*, 2782–2799. [[CrossRef](#)]
10. Dahman, Y.; Deonanan, K.; Dontosos, T.; Iammateo, A. Nanopolymers. In *Nanotechnology and Functional Materials for Engineers*; Elsevier: Amsterdam, The Netherlands, 2017; pp. 121–144. [[CrossRef](#)]
11. Barakat, M.A. New trends in removing heavy metals from industrial wastewater. *Arab. J. Chem.* **2011**, *4*, 361–377. [[CrossRef](#)]
12. Ahmaruzzaman, M. Industrial wastes as low-cost potential adsorbents for the treatment of wastewater laden with heavy metals. *Adv. Colloid Interface Sci.* **2011**, *166*, 36–59. [[CrossRef](#)]
13. Rathi, B.S.; Kumar, P.S. Application of adsorption process for effective removal of emerging contaminants from water and wastewater. *Environ. Pollut.* **2021**, *280*, 116995. [[CrossRef](#)]
14. Hadi, P.; To, M.H.; Hui, C.W.; Lin, C.S.K.; McKay, G. Aqueous mercury adsorption by activated carbons. *Water Res.* **2015**, *73*, 37–55. [[CrossRef](#)] [[PubMed](#)]
15. Božić, D.; Stanković, V.; Gorgievski, M.; Bogdanović, G.; Kovačević, R. Adsorption of heavy metal ions by sawdust of deciduous trees. *J. Hazard. Mater.* **2009**, *171*, 684–692. [[CrossRef](#)] [[PubMed](#)]
16. Park, H.J.; Jeong, S.W.; Yang, J.K.; Kim, B.G.; Lee, S.M. Removal of heavy metals using waste eggshell. *J. Environ. Sci.* **2007**, *19*, 1436–1441. [[CrossRef](#)] [[PubMed](#)]
17. Renu; Agarwal, M.; Singh, S.K. Heavy metal removal from wastewater using various adsorbents: A review. *J. Water Reuse Desalination* **2017**, *7*, 387–419. [[CrossRef](#)]
18. Saxena, A.; Bhardwaj, M.; Allen, T.; Kumar, S.; Sahney, R. Adsorption of heavy metals from wastewater using agricultural–industrial wastes as biosorbents. *Water Sci.* **2017**, *31*, 189–197. [[CrossRef](#)]
19. Threepanich, A.; Praipipat, P. Efficacy study of recycling materials by lemon peels as novel lead adsorbents with comparing of material form effects and possibility of continuous flow experiment. *Environ. Sci. Pollut. Res.* **2022**, *29*, 46077–46090. [[CrossRef](#)]
20. Chu, K.H. Removal of copper from aqueous solution by chitosan in prawn shell: Adsorption equilibrium and kinetics. *J. Hazard. Mater.* **2002**, *90*, 77–95. [[CrossRef](#)]
21. Wan Ngah, W.S.; Teong, L.C.; Hanafiah, M.A.K.M. Adsorption of dyes and heavy metal ions by chitosan composites: A review. *Carbohydr. Polym.* **2011**, *83*, 1446–1456. [[CrossRef](#)]
22. Wang, J.; Chen, C. Chitosan-based biosorbents: Modification and application for biosorption of heavy metals and radionuclides. *Bioresour. Technol.* **2014**, *160*, 129–141. [[CrossRef](#)]
23. Jiang, T.; James, R.; Kumbar, S.G.; Laurencin, C.T. Chitosan as a Biomaterial: Structure, Properties, and Applications in Tissue Engineering and Drug Delivery. In *Natural and Synthetic Biomedical Polymers*; Elsevier Inc.: Amsterdam, The Netherlands, 2014; pp. 91–113. [[CrossRef](#)]
24. Singh, S.; Wasewar, K.L.; Kansal, S.K. Low-cost adsorbents for removal of inorganic impurities from wastewater. In *Inorganic Pollutants in Water*; Elsevier: Amsterdam, The Netherlands, 2020; pp. 173–203. [[CrossRef](#)]
25. Scheinost, A.C. METAL OXIDES. In *Encyclopedia of Soils in the Environment*; Elsevier: Amsterdam, The Netherlands, 2005; pp. 428–438. [[CrossRef](#)]
26. Praipipat, P.; Ngamsurach, P.; Pratumkaew, K. The synthesis, characterizations, and lead adsorption studies of chicken eggshell powder and chicken eggshell powder-doped iron (III) oxide-hydroxide. *Arab. J. Chem.* **2023**, *16*, 104640. [[CrossRef](#)]
27. Praipipat, P.; Ngamsurach, P.; Sanghuayprai, A. Modification of sugarcane bagasse with iron(III) oxide-hydroxide to improve its adsorption property for removing lead(II) ions. *Sci. Rep.* **2023**, *13*, 1467. [[CrossRef](#)]
28. Threepanich, A.; Praipipat, P. Powdered and beaded lemon peels-doped iron (III) oxide-hydroxide materials for lead removal applications: Synthesis, characterizations, and lead adsorption studies. *J. Environ. Chem. Eng.* **2021**, *9*, 106007. [[CrossRef](#)]
29. Praipipat, P.; Ngamsurach, P.; Roopkhan, N. Zeolite A powder and beads from sugarcane bagasse fly ash modified with iron(III) oxide-hydroxide for lead adsorption. *Sci. Rep.* **2023**, *13*, 1873. [[CrossRef](#)]
30. Ngamsurach, P.; Namwongsa, N.; Praipipat, P. Synthesis of powdered and beaded chitosan materials modified with ZnO for removing lead (II) ions. *Sci. Rep.* **2022**, *12*, 17184. [[CrossRef](#)]
31. Ngamsurach, P.; Nemkhuntod, S.; Chanaphan, P.; Praipipat, P. Modified Beaded Materials from Recycled Wastes of Bagasse and Bagasse Fly Ash with Iron(III) Oxide-Hydroxide and Zinc Oxide for the Removal of Reactive Blue 4 Dye in Aqueous Solution. *ACS Omega* **2022**, *7*, 34839–34857. [[CrossRef](#)]
32. Praipipat, P.; Ngamsurach, P.; Saekrathok, C.; Phomtai, S. Chicken and duck eggshell beads modified with iron (III) oxide-hydroxide and zinc oxide for reactive blue 4 dye removal. *Arab. J. Chem.* **2022**, *15*, 104291. [[CrossRef](#)]
33. Praipipat, P.; Ngamsurach, P.; Prasongdee, V. Comparative Reactive Blue 4 Dye Removal by Lemon Peel Bead Doping with Iron(III) Oxide-Hydroxide and Zinc Oxide. *ACS Omega* **2022**, *7*, 41744–41758. [[CrossRef](#)]
34. Praipipat, P.; Ngamsurach, P.; Thanyahan, A.; Sakda, A.; Nitayarat, J. Reactive blue 4 adsorption efficiencies on bagasse and bagasse fly ash beads modified with titanium dioxide (TiO₂), magnesium oxide (MgO), and aluminum oxide (Al₂O₃). *Ind. Crops Prod.* **2023**, *191*, 115928. [[CrossRef](#)]
35. Ouachtak, H.; Akhouairi, S.; Haounati, R.; Addi, A.A.; Jada, A.; Taha, M.L.; Douch, J. 3,4-Dihydroxybenzoic acid removal from water by goethite modified natural sand column fixed-bed: Experimental study and mathematical modeling. *Desalination Water Treat* **2020**, *194*, 439–449. [[CrossRef](#)]
36. Ouachtak, H.; Akhouairi, S.; Ait Addi, A.; Ait Akbour, R.; Jada, A.; Douch, J.; Hamdani, M. Mobility and retention of phenolic acids through a goethite-coated quartz sand column. *Colloids Surf. A Physicochem. Eng. Asp.* **2018**, *546*, 9–19. [[CrossRef](#)]

37. Hua, M.; Zhang, S.; Pan, B.; Zhang, W.; Lv, L.; Zhang, Q. Heavy metal removal from water/wastewater by nanosized metal oxides: A review. *J. Hazard. Mater.* **2012**, *211–212*, 317–331. [[CrossRef](#)]
38. Phuengprasop, T.; Sittiwong, J.; Unob, F. Removal of heavy metal ions by iron oxide coated sewage sludge. *J. Hazard. Mater.* **2011**, *186*, 502–507. [[CrossRef](#)]
39. Shen, L.; Wang, J.; Li, Z.; Fan, L.; Chen, R.; Wu, X.; Li, J.; Zeng, W. A high-efficiency Fe₂O₃@Microalgae composite for heavy metal removal from aqueous solution. *J. Water Process Eng.* **2020**, *33*, 101026. [[CrossRef](#)]
40. Li, Y.; Gao, L.; Lu, Z.; Wang, Y.; Wang, Y.; Wan, S. Enhanced Removal of Heavy Metals from Water by Hydrous Ferric Oxide-Modified Biochar. *ACS Omega* **2020**, *5*, 28702–28711. [[CrossRef](#)] [[PubMed](#)]
41. Nejadshafiee, V.; Islami, M.R. Adsorption capacity of heavy metal ions using sultone-modified magnetic activated carbon as a bio-adsorbent. *Mater. Sci. Eng. C* **2019**, *101*, 42–52. [[CrossRef](#)]
42. Praipipat, P.; Ngamsurach, P.; Kosumphon, S.; Mokkarat, J. Powdered and beaded sawdust materials modified iron (III) oxide-hydroxide for adsorption of lead (II) ion and reactive blue 4 dye. *Sci. Rep.* **2023**, *13*, 531. [[CrossRef](#)] [[PubMed](#)]
43. Praipipat, P.; Jangkorn, S.; Ngamsurach, P. Powdered and beaded zeolite A from recycled coal fly ash with modified iron (III) oxide-hydroxide for lead adsorptions. *Environ. Nanotechnol. Monit. Manag.* **2023**, *20*, 100812. [[CrossRef](#)]
44. Pawar, R.R.; Lallhumsiamia; Kim, M.; Kim, J.G.; Hong, S.M.; Sawant, S.Y.; Lee, S.M. Efficient removal of hazardous lead, cadmium, and arsenic from aqueous environment by iron oxide modified clay-activated carbon composite beads. *Appl. Clay. Sci.* **2018**, *162*, 339–350. [[CrossRef](#)]
45. Singh, J.; Sharma, M.; Basu, S. Heavy metal ions adsorption and photodegradation of remazol black XP by iron oxide/silica monoliths: Kinetic and equilibrium modelling. *Adv. Powder Technol.* **2018**, *29*, 2268–2279. [[CrossRef](#)]
46. Facchi, D.P.; Cazetta, A.L.; Canesin, E.A.; Almeida, V.C.; Bonafé, E.G.; Kipper, M.J.; Martins, A.F. New magnetic chitosan/alginate/Fe₃O₄@SiO₂ hydrogel composites applied for removal of Pb(II) ions from aqueous systems. *Chem. Eng. J.* **2018**, *337*, 595–608. [[CrossRef](#)]
47. Saad, A.H.A.; Azzam, A.M.; El-Wakeel, S.T.; Mostafa, B.B.; Abd El-latif, M.B. Removal of toxic metal ions from wastewater using ZnO@Chitosan core-shell nanocomposite. *Environ. Nanotechnol. Monit. Manag.* **2018**, *9*, 67–75. [[CrossRef](#)]
48. Fan, C.; Li, K.; He, Y.; Wang, Y.; Qian, X.; Jia, J. Evaluation of magnetic chitosan beads for adsorption of heavy metal ions. *Sci. Total Environ.* **2018**, *627*, 1396–1403. [[CrossRef](#)] [[PubMed](#)]
49. Varun, T.K.; Senani, W.; Kumar, N.; Gautam, M.; Gupta, R.; Gupta, M. Extraction and characterization of chitin, chitosan and chitooligosaccharides from crab shell waste. *Indian J. Anim. Res.* **2017**, *51*, 1066–1072. [[CrossRef](#)]
50. Boudouaia, N.; Bengharez, Z.; Jellali, S. Preparation and characterization of chitosan extracted from shrimp shells waste and chitosan film: Application for Eriochrome black T removal from aqueous solutions. *Appl. Water Sci.* **2019**, *9*, 91. [[CrossRef](#)]
51. De Queiroz Antonino, R.S.C.M.; Lia Fook, B.R.P.; De Oliveira Lima, V.A.; De Farias Rached, R.Í.; Lima, E.P.N.; Da Silva Lima, R.J.; Peniche Covas, C.A.; Lia Fook, M.V. Preparation and characterization of chitosan obtained from shells of shrimp (*Litopenaeus vannamei* Boone). *Mar. Drugs* **2017**, *15*, 141. [[CrossRef](#)]
52. Maneechakr, P.; Karnjanakom, S. Facile utilization of magnetic MnO₂@Fe₃O₄@sulfonated carbon sphere for selective removal of hazardous Pb(II) ion with an excellent capacity: Adsorption behavior/isotherm/kinetic/thermodynamic studies. *J. Environ. Chem. Eng.* **2021**, *9*, 106191. [[CrossRef](#)]
53. Jangkorn, S.; Youngme, S.; Praipipat, P. Comparative lead adsorptions in synthetic wastewater by synthesized zeolite A of recycled industrial wastes from sugar factory and power plant. *Heliyon* **2022**, *8*, e09323. [[CrossRef](#)]
54. Sing, K.S.W. Characterization Of Porous Solids: An Introductory Survey. In *Studies in Surface Science and Catalysis*; Rodriguez-Reinoso, F., Rouquerol, J., Sing, K.S.W., Unger, K.K., Eds.; Elsevier: Amsterdam, The Netherlands, 1991; pp. 1–9. [[CrossRef](#)]
55. Chagas, P.M.B.; de Carvalho, L.B.; Caetano, A.A.; Nogueira, F.G.E.; Corrêa, A.D.; do Rosário Guimarães, I. Nanostructured oxide stabilized by chitosan: Hybrid composite as an adsorbent for the removal of chromium (VI). *J. Environ. Chem. Eng.* **2018**, *6*, 1008–1019. [[CrossRef](#)]
56. Tong, Z.; Chen, Y.; Liu, Y.; Tong, L.; Chu, J.; Xiao, K.; Zhou, Z.; Dong, W.; Chu, X. Preparation, characterization and properties of alginate/poly(γ -glutamic acid) composite microparticles. *Mar. Drugs* **2017**, *15*, 91. [[CrossRef](#)]
57. Ghanbariasad, A.; Taghizadeh, S.M.; Show, P.L.; Nomanbhay, S.; Berenjian, A.; Ghasemi, Y.; Ebrahiminezhad, A. Controlled synthesis of iron oxyhydroxide (FeOOH) nanoparticles using secretory compounds from *Chlorella vulgaris* microalgae. *Bioengineered* **2019**, *10*, 390–396. [[CrossRef](#)]
58. Munagapati, V.S.; Kim, D.S. Equilibrium isotherms, kinetics, and thermodynamics studies for congo red adsorption using calcium alginate beads impregnated with nano-goethite. *Ecotoxicol. Environ. Saf.* **2017**, *141*, 226–234. [[CrossRef](#)] [[PubMed](#)]
59. Eddy, M.; Tbib, B.; EL-Hami, K. A comparison of chitosan properties after extraction from shrimp shells by diluted and concentrated acids. *Heliyon* **2020**, *6*, e03486. [[CrossRef](#)] [[PubMed](#)]
60. Ngah, W.S.W.; Fatinathan, S. Pb(II) biosorption using chitosan and chitosan derivatives beads: Equilibrium, ion exchange and mechanism studies. *J. Environ. Sci.* **2010**, *22*, 338–346. [[CrossRef](#)]
61. Munagapati, V.S.; Yarramuthi, V.; Kim, D.S. Methyl orange removal from aqueous solution using goethite, chitosan beads and goethite impregnated with chitosan beads. *J. Mol. Liq.* **2017**, *240*, 329–339. [[CrossRef](#)]
62. Ablouh, E.H.; Essaghraoui, A.; Eladlani, N.; Rhazi, M.; Taourirte, M. Uptake of pb(II) onto nanochitosan/sodium alginate hybrid beads: Mechanism and kinetics study. *Water Environ. Res.* **2019**, *91*, 239–249. [[CrossRef](#)]

63. Ablouh, E.H.; Hanani, Z.; Eladlani, N.; Rhazi, M.; Taourirte, M. Chitosan microspheres/sodium alginate hybrid beads: An efficient green adsorbent for heavy metals removal from aqueous solutions. *Sustain. Environ. Res.* **2019**, *29*, 5. [[CrossRef](#)]
64. Churio, O.; Pizarro, F.; Valenzuela, C. Preparation and characterization of iron-alginate beads with some types of iron used in supplementation and fortification strategies. *Food Hydrocoll.* **2018**, *74*, 1–10. [[CrossRef](#)]
65. Rahimi, S.; Moattari, R.M.; Rajabi, L.; Derakhshan, A.A. Optimization of lead removal from aqueous solution using goethite/chitosan nanocomposite by response surface methodology. *Colloids Surf. A Physicochem. Eng. Asp.* **2015**, *484*, 216–225. [[CrossRef](#)]
66. Kalyani, S.; Priya, J.A.; Rao, P.S.; Krishnaiah, A. Removal of copper and nickel from aqueous solutions using chitosan coated on perlite as biosorbent. *Sep. Sci. Technol.* **2005**, *40*, 1483–1495. [[CrossRef](#)]
67. Chen, Y.; Nie, Z.; Gao, J.; Wang, J.; Cai, M. A novel adsorbent of bentonite modified chitosan-microcrystalline cellulose aerogel prepared by bidirectional regeneration strategy for Pb(II) removal. *J. Environ. Chem. Eng.* **2021**, *9*, 105755. [[CrossRef](#)]
68. Ekayem, N.A.; Alhwaige, A.A.; Elhrari, W.; Amer, M. Removal of lead (II) ions from water using chitosan/polyester crosslinked spheres derived from chitosan and glycerol-based polyester. *J. Environ. Chem. Eng.* **2021**, *9*, 106628. [[CrossRef](#)]
69. Nurchi, V.M.; Villaescus, I. The Chemistry Behind the Use of Agricultural Biomass as Sorbent for Toxic Metal Ions: pH Influence, Binding Groups, and Complexation Equilibria. In *Biomass—Detection, Production and Usage*; InTech: London, UK, 2011. [[CrossRef](#)]
70. Wang, X.; Wang, L.; Wang, Y.; Tan, R.; Ke, X.; Zhou, X.; Geng, J.; Hou, H.; Zhou, M. Calcium Sulfate Hemihydrate Whiskers Obtained from Flue Gas Desulfurization Gypsum and Used for the Adsorption Removal of Lead. *Crystals* **2017**, *7*, 270. [[CrossRef](#)]
71. Kovačević, D.; Pohlmeier, A.; Özbaş, G.; Narres, H.-D.; Kallay, M.J.N. The adsorption of lead species on goethite. *Colloids Surf. A Physicochem. Eng. Asp.* **2000**, *166*, 225–233. [[CrossRef](#)]
72. Adegoke, H.; Adekola, F.; Fatoki, O.; Ximba, B. Sorptive Interaction of Oxyanions with Iron Oxides: A Review. *Pol. J. Environ. Stud.* **2013**, *22*, 7–24.
73. Kosmulski, M. The pH dependent surface charging and points of zero charge. VII. Update. *Adv. Colloid Interface Sci.* **2018**, *251*, 115–138. [[CrossRef](#)] [[PubMed](#)]
74. Bugarčić, M.; Lopičić, Z.; Šoštarić, T.; Marinković, A.; Rusmirovic, J.D.; Milošević, D.; Milivojević, M. Vermiculite enriched by Fe(III) oxides as a novel adsorbent for toxic metals removal. *J. Environ. Chem. Eng.* **2021**, *9*, 106020. [[CrossRef](#)]
75. Hu, C.; Zhu, P.; Cai, M.; Hu, H.; Fu, Q. Comparative adsorption of Pb(II), Cu(II) and Cd(II) on chitosan saturated montmorillonite: Kinetic, thermodynamic and equilibrium studies. *Appl. Clay Sci.* **2017**, *143*, 320–326. [[CrossRef](#)]
76. Christopher, F.C.; Anbalagan, S.; Kumar, P.S.; Pannerselvam, S.R.; Vaidyanathan, V.K. Surface adsorption of poisonous Pb(II) ions from water using chitosan functionalised magnetic nanoparticles. *IET Nanobiotechnol.* **2017**, *11*, 433–442. [[CrossRef](#)] [[PubMed](#)]
77. Sahoo, T.R.; Prelot, B. Adsorption processes for the removal of contaminants from wastewater: The perspective role of nanomaterials and nanotechnology. In *Nanomaterials for the Detection and Removal of Wastewater Pollutants*; Elsevier: Amsterdam, The Netherlands, 2020; pp. 161–222. [[CrossRef](#)]
78. Mahmoud, M.E.; Saleh, M.M.; Zaki, M.M.; Nabil, G.M. A sustainable nanocomposite for removal of heavy metals from water based on crosslinked sodium alginate with iron oxide waste material from steel industry. *J. Environ. Chem. Eng.* **2020**, *8*, 104015. [[CrossRef](#)]
79. Sabbagh, N.; Tahvildari, K.; Mehrdad Sharif, A.A. Application of chitosan-alginate bio composite for adsorption of malathion from wastewater: Characterization and response surface methodology. *J. Contam. Hydrol.* **2021**, *242*, 103868. [[CrossRef](#)]
80. Kang, Y.G.; Vu, H.C.; Le, T.T.; Chang, Y.S. Activation of persulfate by a novel Fe(II)-immobilized chitosan/alginate composite for bisphenol A degradation. *Chem. Eng. J.* **2018**, *353*, 736–745. [[CrossRef](#)]

Disclaimer/Publisher’s Note: The statements, opinions and data contained in all publications are solely those of the individual author(s) and contributor(s) and not of MDPI and/or the editor(s). MDPI and/or the editor(s) disclaim responsibility for any injury to people or property resulting from any ideas, methods, instructions or products referred to in the content.